Since January 2020 Elsevier has created a COVID-19 resource centre with free information in English and Mandarin on the novel coronavirus COVID-19. The COVID-19 resource centre is hosted on Elsevier Connect, the company's public news and information website.

Cell Reports

Article

mRNA-encoded HIV-1 Env trimer ferritin nanoparticles induce monoclonal antibodies that neutralize heterologous HIV-1 isolates in mice

Graphical abstract

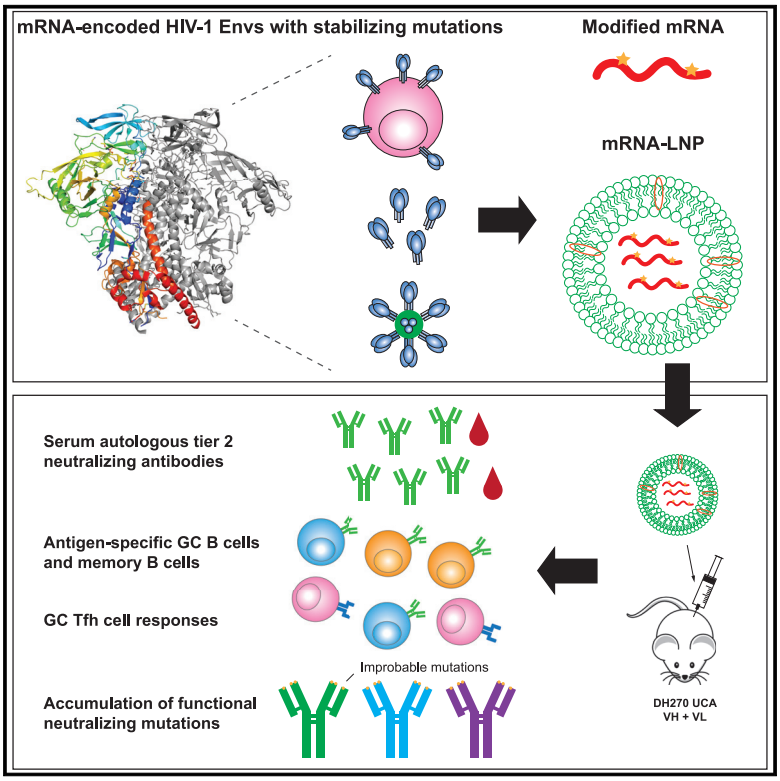

Highlights

- mRNA-expressed HIV-1 Envs are well folded with optimal stabilizing mutations
- mRNA-expressed stabilized Envs show preferential bnAb binding
- mRNA-LNP elicit autologous tier 2 neutralizing antibodies with key bnAb mutations
- Induced monoclonal antibodies with key mutations neutralize heterologous viruses

Authors

Zekun Mu, Kevin Wiehe, Kevin O. Saunders, ..., Norbert Pardi, Drew Weissman, Barton F. Haynes

Correspondence

barton.haynes@duke.edu (B.F.H.), zekun.mu@duke.edu (Z.M.), dreww@pennmedicine.upenn.edu (D.W.)

In brief

mRNA vaccines are highly effective against COVID-19. Mu et al. demonstrate the use of mRNA to express HIV-1 Env trimers scaffolded on ferritin nanoparticles. mRNA vaccination in mice induced autologous tier 2 neutralizing antibodies and key functional mutations. Isolated monoclonal antibodies neutralized heterologous HIV-1 isolates.

Mu et al., 2022, Cell Reports *38*, 110514
March 15, 2022
https://doi.org/10.1016/j.celrep.2022.110514

CellPress

Cell Reports

CellPress
OPEN ACCESS

Article

mRNA-encoded HIV-1 Env trimer ferritin nanoparticles induce monoclonal antibodies that neutralize heterologous HIV-1 isolates in mice

Zekun Mu,[1,2,*] Kevin Wiehe,[2,3] Kevin O. Saunders,[1,2,4,5] Rory Henderson,[2,3] Derek W. Cain,[2] Robert Parks,[2] Diana Martik,[2] Katayoun Mansouri,[2] Robert J. Edwards,[2,3] Amanda Newman,[2] Xiaozhi Lu,[2] Shi-Mao Xia,[2] Amanda Eaton,[2] Mattia Bonsignori,[2,3,10] David Montefiori,[2,4] Qifeng Han,[2,11] Sravani Venkatayogi,[2] Tyler Evangelous,[2] Yunfei Wang,[2] Wes Rountree,[2] Bette Korber,[6] Kshitij Wagh,[6] Ying Tam,[7] Christopher Barbosa,[7] S. Munir Alam,[2] Wilton B. Williams,[1,2,4] Ming Tian,[8] Frederick W. Alt,[9] Norbert Pardi,[9] Drew Weissman,[9,*] and Barton F. Haynes[1,2,3,12,*]

[1]Department of Immunology, Duke University School of Medicine, Durham, NC 27710, USA
[2]Duke Human Vaccine Institute, Duke University School of Medicine, Durham, NC 27710, USA
[3]Department of Medicine, Duke University School of Medicine, Durham, NC 27710, USA
[4]Department of Surgery, Duke University School of Medicine, Durham, NC 27710, USA
[5]Department of Molecular Genetics and Microbiology, Duke University School of Medicine, Durham, NC 27710, USA
[6]Theoretical Biology and Biophysics, Los Alamos National Laboratory, Los Alamos, NM 87545, USA
[7]Acuitas, Inc, Vancouver, Canada
[8]Howard Hughes Medical Institute, Program in Cellular and Molecular Medicine, Boston Children's Hospital, Department of Genetics, Harvard Medical School, Boston, MA 02115, USA
[9]Perelman School of Medicine, University of Pennsylvania, Philadelphia, PA 19104, USA
[10]Present address: Translational Immunobiology Unit, Laboratory of Infectious Diseases, National Institute of Allergy and Infectious Diseases, National Institutes of Health, Bethesda, MD 20892, USA
[11]Present address: Novo Nordisk Research Center China, Novo Nordisk A/S, Beijing 102206, China
[12]Lead contact
*Correspondence: barton.haynes@duke.edu (B.F.H.), zekun.mu@duke.edu (Z.M.), dreww@pennmedicine.upenn.edu (D.W.)
https://doi.org/10.1016/j.celrep.2022.110514

SUMMARY

The success of nucleoside-modified mRNAs in lipid nanoparticles (mRNA-LNP) as COVID-19 vaccines heralded a new era of vaccine development. For HIV-1, multivalent envelope (Env) trimer protein nanoparticles are superior immunogens compared with trimers alone for priming of broadly neutralizing antibody (bnAb) B cell lineages. The successful expression of complex multivalent nanoparticle immunogens with mRNAs has not been demonstrated. Here, we show that mRNAs can encode antigenic Env trimers on ferritin nanoparticles that initiate bnAb precursor B cell expansion and induce serum autologous tier 2 neutralizing activity in bnAb precursor V_H + V_L knock-in mice. Next-generation sequencing demonstrates acquisition of critical mutations, and monoclonal antibodies that neutralize heterologous HIV-1 isolates are isolated. Thus, mRNA-LNP can encode complex immunogens and may be of use in design of germline-targeting and sequential boosting immunogens for HIV-1 vaccine development.

INTRODUCTION

Nucleoside-modified mRNA COVID-19 vaccines encoding SARS-CoV-2 trimeric spike protein have demonstrated the robust nature of mRNA vaccines (Baden et al., 2020; Polack et al., 2020; Sahin et al., 2020). In addition to success with clinically-approved COVID-19 spike trimer vaccines, pre-clinical success has been demonstrated with nucleoside-modified mRNA encapsulated in lipid nanoparticle (mRNA-LNP) expression of Zika prM-E (Pardi et al., 2017), influenza hemagglutinin (Pardi et al., 2018a, 2018b), and HIV-1 envelope (Env) in gp120 monomers or gp140 trimers (; Pardi et al., 2018a; Saunders et al., 2021). However, recent studies have shown that protein trimer nanoparticle (NP) multimers may be advantageous as immunogens (Abbott et al., 2018; Havenar-Daughton et al., 2018; Kato et al., 2020; Saunders et al., 2019; Tokatlian et al., 2019).

HIV-1 broadly neutralizing antibodies (bnAbs) may be disfavored by the immune system due to their characteristics of long heavy-chain complementarity-determining region 3 (HCDR3) loops and polyreactivity or autoreactivity that predispose bnAbs to immune tolerance control (Havenar-Daughton et al., 2018; Haynes et al., 2005, 2012, 2016, 2019; Huang et al., 2020; Moody et al., 2016; Saunders et al., 2019; Steichen et al., 2019; Zhang et al., 2016). Thus, the biology of HIV-1 bnAbs has necessitated a strategy whereby the unmutated common ancestor (UCA) or germline (GL) precursor of bnAb B cell lineage is targeted with priming immunogens to expand the bnAb precursor pool (Haynes et al., 2012, 2019;

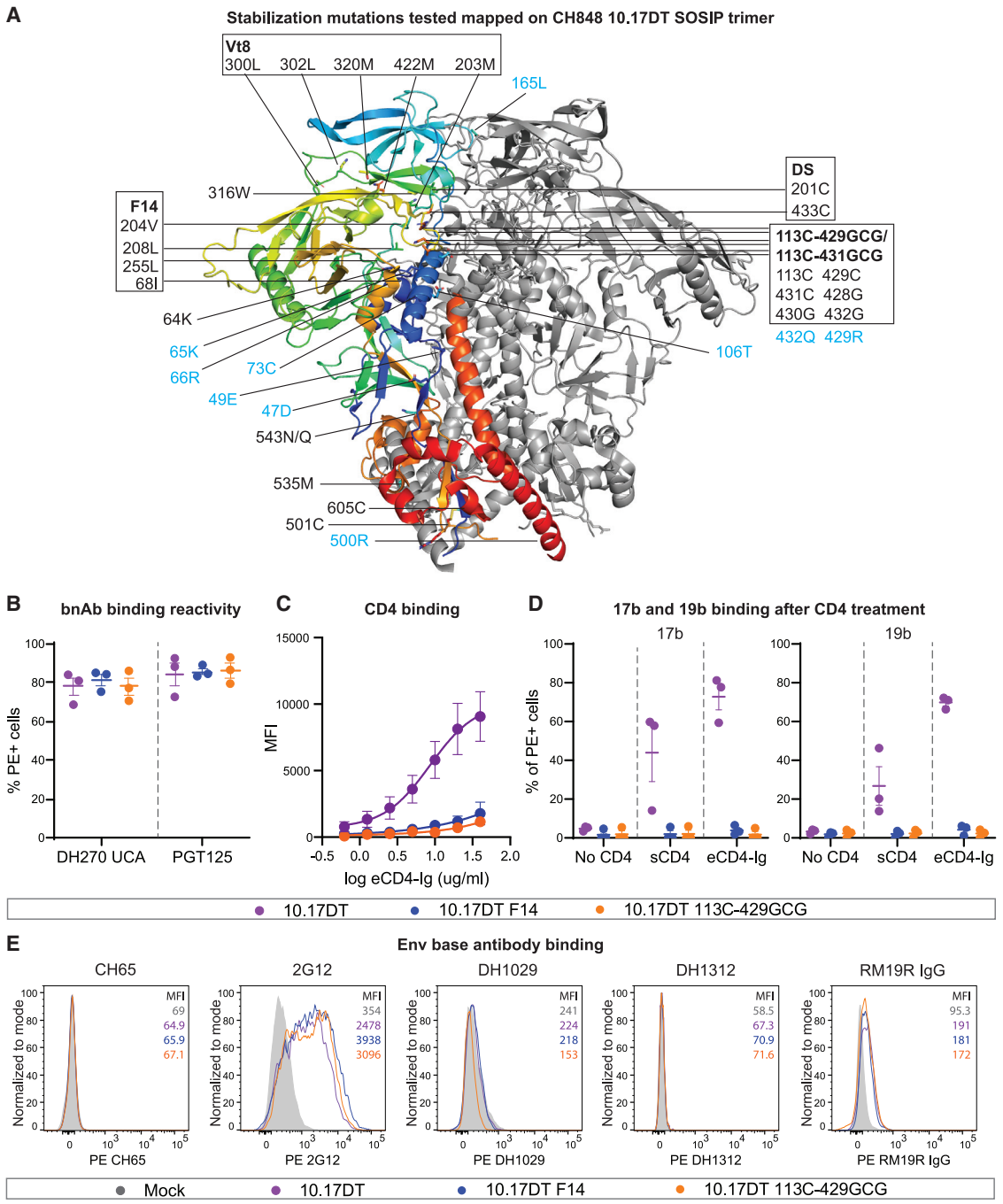

Figure 1. Antigenicity of modified mRNA-encoded CH848 10.17DT gp160 with stabilizing mutations

(A) Stabilizing mutations tested in this study mapped onto structure of CH848 10.17DT SOSIP trimer (PDB ID: 6UM5). One protomer is shown in rainbow color, and the other two protomers are shown in gray. Amino acid mutations are listed in boxes. Black fonts outside of boxes are mutations in v4.1, and blue fonts are mutations in v5.2.8, in addition to v4.1 mutations. Residue 561C in v5.2.8 or redesigned HR1 region in UFO mutation is not shown due to lack of HR1 region in this structure.

(B) Antigenicity of mRNA-expressed CH848 10.17DT, F14, and 113C-429GCG transmembrane gp160s measured by binding of bnAb PGT125 and DH270 UCA. Data are shown as means ± standard error of the mean (SEM) of Phycoerythrin + (PE +) cell percentage among live cells from three independent experiments.

(C) eCD4-Ig binding reactivity to mRNA-expressed CH848 10.17DT, F14, and 113C-429GCG gp160s. Data shown are averages of mean fluorescent intensity (MFI) from three independent experiments. Error bars, means ± SEM.

(legend continued on next page)

Jardine et al., 2013; McGuire et al., 2013). Env immunogens designed to select for key antibody mutations, administered in a specific order, are postulated to be able to guide antibody affinity maturation toward bnAb breadth and potency (Bonsignori et al., 2016, 2017; Havenar-Daughton et al., 2018; Haynes et al., 2012, 2016, 2019; Huang et al., 2020; Saunders et al., 2019; Steichen et al., 2019; Zhang et al., 2016). However, guiding bnAb development is difficult, because HIV-1 bnAbs are enriched in improbable functional somatic mutations that are required for neutralization potency and breadth (Bonsignori et al., 2017; Wiehe et al., 2018). Rare somatic mutations are due to lack of targeting by the somatic mutation enzyme activation-induced cytidine deaminase (AID). To promote bnAb development, Envs will need to engage B cell receptors that have accumulated functional improbable mutations, thereby selecting intermediate bnAb B cell lineage members to proliferate and evolve further (Bonsignori et al., 2017; Haynes et al., 2012; Wiehe et al., 2018). Whereas bnAbs arise in ~50% of HIV-1-infected individuals (Hraber et al., 2014), to date, potent and durable bnAbs have not been induced in humans by vaccination.

HIV-1 Env is metastable and can adopt open and closed conformations (Tran et al., 2012; Ward and Wilson, 2017). The Env open conformation exposes non-neutralizing antibody (nnAb) epitopes that can create competition for Env antigen between nnAb and bnAb precursors (Havenar-Daughton et al., 2017; Lee et al., 2021; McGuire et al., 2014). To address the problem of Env trimer opening and the exposure of non-neutralizing epitopes, multiple strategies have been designed to stabilize Env trimers in native-like conformations (de Taeye et al., 2015; Guenaga et al., 2015; Henderson et al., 2020; Kong et al., 2016). However, whether stabilizing mutations for mRNA expression of complex multimers will result in the desired antigenicity and immunogenicity of trimer multimer NPs is not known.

We have previously demonstrated that a HIV-1 Env trimer, CH848, with two glycosylation sites in the first variable region (V1), eliminated (CH848 N133D N138T, CH848 10.17DT), conjugated to a ferritin nanoparticle that was superior to the Env trimer alone as an immunogen, and was capable of initiating a V3-glycan bnAb lineage with key improbable mutations in bnAb UCA heavy- and light-chain variable regions (V_H + V_L) knock-in (KI) mice (Saunders et al., 2019).

Here, we determined stabilizing mutations in the CH848 10.17DT immunogen for formulation as mRNA-LNP. We demonstrated that modified mRNA Env expression resulted in Env binding to bnAbs in the forms of transmembrane gp160s, soluble gp140 SOSIP trimers, or SOSIP trimer-ferritin NPs encoded by mRNA (trimer-ferritin NPs, hereafter "NPs"). Moreover, we demonstrated that immunization of bnAb UCA V_H + V_L KI mice with mRNA-LNP encoding CH848 10.17DT gp160s or NPs initiated a V3-glycan bnAb B cell lineage, selected for bnAb lineage B cells with B cell receptors (BCRs) bearing functional improbable mutations and induced high serum titers of tier 2 V3-glycan bnAb N332-dependent autologous neutralizing antibodies.

RESULTS

Antigenicity of modified mRNA-encoded CH848 10.17DT gp160s with stabilizing mutations

We studied ten stabilization designs in CH848 10.17DT Env for expression as mRNAs (de Taeye et al., 2015; Guenaga et al., 2015; Henderson et al., 2020; Kong et al., 2016; Tran et al., 2012; Ward and Wilson, 2017; Zhang et al., 2018) (Figure 1A and Table S1; see STAR methods).We first designed mRNAs with stabilizing mutations encoding CH848 10.17DT Envs as transmembrane gp160s (Table S1). All mRNA constructs expressed and showed robust V3-glycan bnAb binding (Figure S1). In particular, CH848 10.17DT F14, 113C-429GCG, and 113C-431GCG gp160s exhibited binding reactivity to mature V3-glycan bnAb PGT125 and the DH270 UCA equal to that of 10.17DT gp160 without stabilizing mutations (Figure 1B). In contrast, DS, Vt8, and F14/Vt8 mutations decreased DH270 UCA binding to 10.17DT gp160s (Figure S1B).

To evaluate expression of CD4-induced (CD4i) Env epitopes, we examined the susceptibility of each Env gp160 to CD4 triggering in transfected 293-F cells. Engineered CD4-Ig (eCD4-Ig) (Fellinger et al., 2019) bound to CH848 10.17DT gp160 lacking stabilizing mutations in a dose-dependent manner, but binding to 10.17DT F14 and 113C-429GCG gp160s was minimal (Figure 1C). Next, we assessed whether mutations could stabilize 10.17DT gp160s in prefusion conformations and prevent V3 loop or C-C chemokine receptor type 5 (CCR5) co-receptor binding site exposure. mRNA-transfected 293-F cells were either untreated or treated with 20 μg/mL of sCD4, eCD4-Ig, or CD4-IgG2 (Allaway et al., 1995), and Env conformation was determined by binding of CCR5 co-receptor binding site nnAb, 17b or distal V3 loop nnAb, 19b. In the absence of CD4 treatment, Env gp160s lacked binding to 17b or 19b. After treatment with sCD4, eCD4-Ig, or CD4-IgG2, 10.17DT gp160 without stabilizing mutations exhibited increased binding to both nnAbs 17b and 19b. In contrast, stabilizing the Env gp160s with F14 or 113C-429GCG mutations completely prevented CD4-induced exposure of 17b and 19b epitopes (Figures 1D and S1C). F14 and 113C-429GCG mutations are outside of the 17b and 19b binding site; thus, these mutations themselves do not interfere with 17b or 19b binding (Henderson et al., 2020; Zhang et al., 2018). In addition, if F14 mutations themselves impair 17b or 19b binding, then similar effects would be observed for any Env strains. Thus, we performed surface plasmon resonance (SPR) analysis of 17b and 19b binding to 10.17DT F14 and CH505 M5 G458Y F14 SOSIP proteins. Some increase to 19b binding was observed with 10.17DT F14 SOSIP after sCD4 treatment. In contrast, robust 19b binding to CH505 M5 G458Y F14

(D) Binding reactivity of nnAbs 17b and 19b to mRNA-expressed CH848 10.17DT, F14, and 113C-429GCG gp160s with or without treatment with sCD4 and eCD4-Ig. Data shown are means ± SEM of PE + cell percentage among live cells from three independent experiments.
(E) Binding of Env base antibodies to mRNA-encoded CH848 10.17DT, F14, and 113C-429GCG gp160s. Anti-Influenza hemagglutinin mAb CH65 was used as negative control, and 2G12 was used as positive control to show gp160 expression. Histograms shown are representative from three independent experiments.
See also Figures S1 and S2 and Table S1.

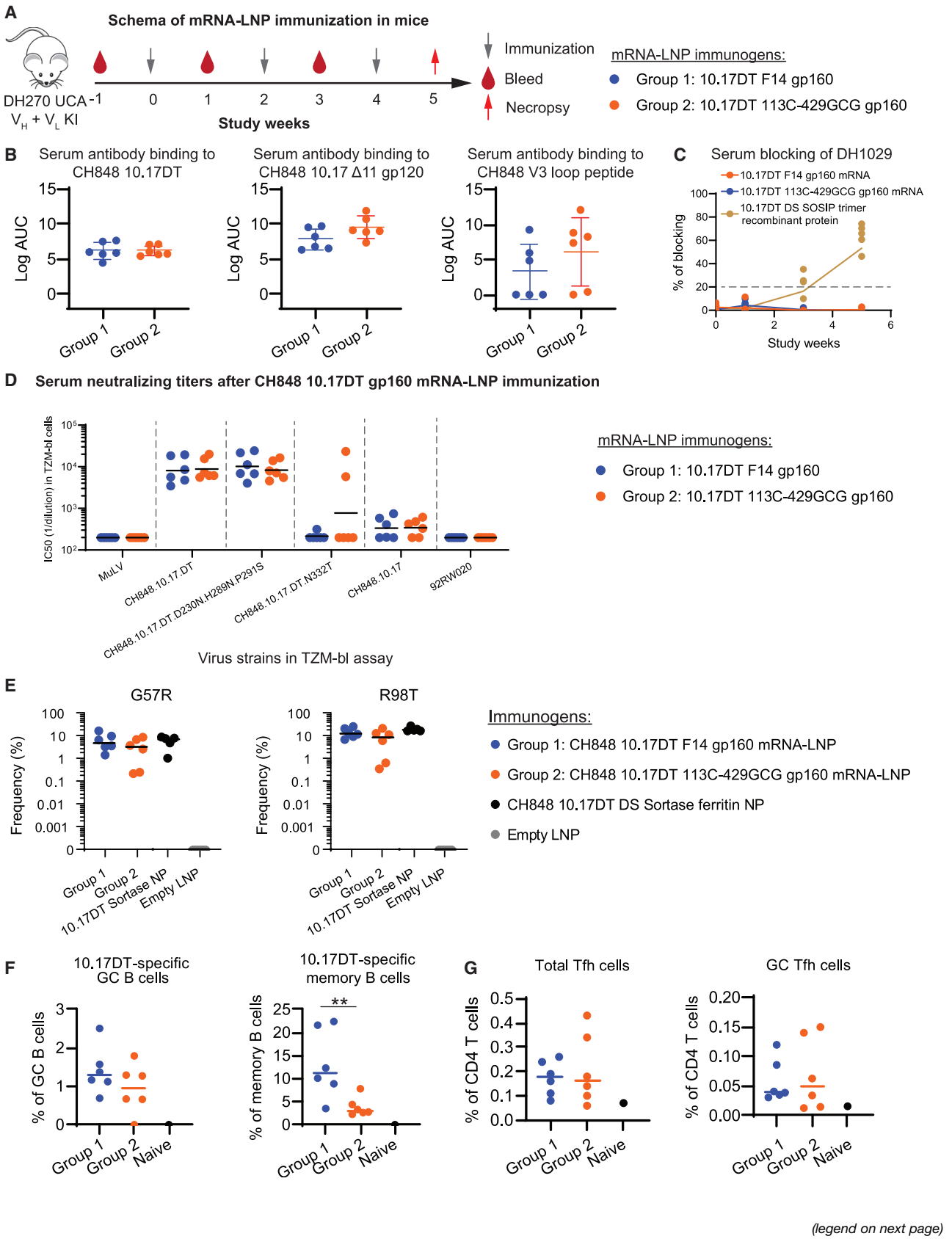

(legend on next page)

SOSIP was observed with or without sCD4 (Figure S1E), demonstrating that F14 mutations do not intrinsically impair 17b or 19b binding. Additionally, anti-gp41 nnAb 7B2 against the immunodominant epitope of gp41 (Pincus et al., 2003) showed low binding to mRNA-expressed 10.17DT Env gp160s, confirming minimal exposure of this gp41 epitope (Figure S1C).

Next, we determined whether expressing Env trimers as transmembrane gp160s resulted in trimer base exposure (Turner et al., 2021). Binding of three Env base antibodies, DH1029, DH1312, and RM19R IgG were tested (Cottrell et al., 2020; Martin et al., 2020). Here, we report the negative-stain electron microscopy (NSEM) structures of DH1029 and DH1312 (Figure S2). We did not observe binding of neither DH1029 nor DH1312 antibodies and observed only minimal binding of RM19R IgG to mRNA-expressed CH848 10.17DT, 10.17DT F14, or 113C-429GCG gp160s (Figures 1E and S1D). Thus, 10.17DT F14 and 113C-429GCG gp160s were stabilized such that they preferentially bound to bnAbs versus nnAbs, had minimal non-neutralizing epitope exposure after CD4 triggering, and limited exposure of the trimer base.

CH848 10.17DT gp160 mRNA-LNP elicited autologous tier 2 neutralizing antibodies *in vivo*

On the basis of stability and antigenicity, we selected CH848 10.17DT F14 and 113C-429GCG gp160s to test their immunogenicity in heterozygous V3-glycan bnAb DH270 UCA heavy- and light-chain ($V_H^{+/-}$, $V_L^{+/-}$) knock-in (DH270 UCA KI) mice (Saunders et al., 2019). mRNAs encoding 10.17DT F14 or 113C-429GCG gp160s were encapsulated in LNP for immunization (Figure 2A). Mice immunized with 10.17DT F14 or 113C-429GCG gp160 mRNA-LNP developed serum-binding IgGs to 10.17DT trimer and gp120 monomer (Figures 2B, S3A, and S3B). Three 10.17DT F14- and four 113C-429GCG gp160 mRNA-LNP-vaccinated mice had IgGs binding to the linear CH848 V3 peptide epitope, indicating low levels of V3 loop exposure *in vivo* (Figures 2B and S3C). We observed non-detectable levels of binding to gp41 in both groups of mice, suggesting that the gp41 on stabilized 10.17DT gp160 Env was not immunogenic *in vivo* (Figure S3D). As confirmation of no relevant exposure of the Env base on 10.17DT F14 or 113C-429GCG gp160s, no DH1029 serum blocking activity was detected (Figure 2C). Both types of stabilized Env gp160 mRNA-LNP immunization induced serum binding IgGs to 10.17DT, 10.17DT F14 and 113C-429GCG gp160s on the surface of transfected 293-F cells (Figure S3F).

Next, we asked whether CH848 10.17DT F14 and 113C-429GCG gp160 mRNA-LNP immunization in DH270 UCA KI mice elicited serum neutralizing antibodies. Neutralizing antibody titers 1 week after the third immunization (week 5) were assessed with a panel of seven pseudotyped HIV-1 strains sensitive to either DH270 UCA or DH270 intermediate antibody 4 (DH270 IA4) (Bonsignori et al., 2017; Saunders et al., 2019) (Figures 2D and S3G). CH848 10.17DT F14 and 113C-429GCG gp160 mRNA-LNP elicited autologous tier 2 neutralizing antibodies against CH848 10.17DT pseudovirus, with ID_{50} geometric mean titers (GMT) of 8103 and 8812, respectively. Neutralization was dependent on V3-glycan at position N332 in all 10.17DT F14 and four out of six 10.17DT 113C-429GCG-vaccinated mice, demonstrating the elicitation of bnAb V3-glycan autologous neutralizing antibodies. Lower titers of neutralizing antibodies against the V1-glycans restored CH848 10.17 virus were observed. Strain-specific holes in glycan shield can elicit glycan hole-targeted autologous tier 2 neutralizing antibodies (Bradley et al., 2016; Crooks et al., 2015; McCoy et al., 2016). Computational prediction (Wagh et al., 2018) identified potential glycan holes at positions 230 and 289 on CH848 10.17 Env (Figure S3E). We constructed a glycan holes filled CH848 10.17DT mutant with amino acid mutations D230N H289N, as well as P291S. Comparable neutralization titers were observed against CH848 10.17DT D230N H289N P291S virus, indicating that most neutralizing antibodies elicited by vaccination were not targeted to glycan holes.

CH848 10.17DT gp160 mRNA-LNP selected for key DH270 bnAb mutations and elicited germinal center responses

Next, splenocytes from 1 week after the third immunization (week 5) were subjected to next-generation sequencing (NGS)

Figure 2. Immunogenicity of CH848 10.17DT gp160 mRNA-LNP in mice

(A) Immunization schema in DH270 UCA KI mice with CH848 10.17DT F14 and 113C-429GCG gp160 mRNA-LNP.

(B) Week 5 serum IgG binding to CH848 10.17DT SOSIP trimer, 10.17 Δ11 gp120, and V3 loop peptide measured by ELISA. Data shown are log-transformed area under the curve (logAUC). Each dot represents an individual mouse (n = 6 each group). Error bar, mean ± standard deviation (SD). No significant statistical difference was observed between two groups ($p > 0.05$).

(C) Measurement of serum IgG that block DH1029 binding to CH848 10.17DT SOSIP trimer. Sera from a group of 10.17DT DS SOSIP trimer protein immunized mice were used to show the induction of base-binding antibodies after SOSIP trimer immunization. Dotted horizontal line indicates background cut-off at 20% blocking.

(D) Week 5 serum neutralizing antibody titers measured in TZM-bl reporting cells with a panel of autologous and heterologous tier 2 HIV-1 pseudoviruses. Murine leukemia virus (MuLV) was used as negative control. Neutralization titers are reported as ID_{50}. Each dot signifies an individual mouse. Horizontal bar, ID_{50} GMT. No significant statistical difference was observed between the two groups ($p > 0.05$).

(E) Improbable G57R and R98T mutation frequencies in DH270 V_H KI gene after CH848 10.17DT gp160 mRNA-LNP immunization. Frequencies were compared to 10.17DT DS Sortase ferritin NP protein immunization and empty LNP immunization. Each dot represents an individual mouse. Horizontal bar, median.

(F) CH848 10.17DT gp160 mRNA-LNP vaccination induced GC B cell responses in spleens. Frequencies of 10.17DT-specific GC B cells among total GC B cells and 10.17DT-specific memory B cells among total memory B cells in splenocytes of CH848 10.17DT F14 or 10.17DT 113C-429GCG gp160 mRNA-LNP vaccinated DH270 UCA KI mice are shown. Each dot represents an individual mouse. Horizontal bar: mean. $^{**}P < 0.01$.

(G) CH848 10.17DT gp160 mRNA-LNP vaccination induced GC Tfh cell responses in spleen. Frequencies of total Tfh and GC Tfh cells among $CD4^+$ T cells in splenocytes after 10.17DT F14 or 113C-429GCG gp160 mRNA-LNP vaccination in DH270 UCA KI mice were assessed by flow cytometry. Each dot represents an individual mouse. Horizontal bar, mean. No significant statistical difference was observed between the two groups ($p > 0.05$). Significance was determined using Exact Wilcoxon Mann-Whitney U test.

See also Figures S3, S4, and S10.

analysis. Both CH848 10.17DT F14 and 113C-429GCG gp160 mRNA-LNP selected the critical improbable G57R mutation in the DH270 UCA V_H KI gene that is necessary for the V3-glycan bnAb B cell lineage to acquire heterologous neutralization breadth (Bonsignori et al., 2017; Wiehe et al., 2018), with the medians of mutation frequency at 5.4% and 3.4%, respectively. Induced antibodies also acquired a second key improbable V_H R98T mutation. Frequencies of the improbable V_H G57R and the R98T mutations were comparable to those in a group of DH270 UCA KI mice immunized with sortase-ligated 10.17DT DS Env ferritin NP protein (Figure 2E; $p > 0.05$, exact Wilcoxon Mann-Whitney U test). Thus, in DH270 UCA KI mice, 10.17DT gp160 mRNA-LNP were immunogenic, induced potent N332-dependent autologous tier 2 neutralizing antibodies, and selected DH270 antibodies that acquired improbable mutations required for acquisition of heterologous HIV-1 neutralization.

Splenocytes from week 5 were phenotyped for germinal center (GC) responses by flow cytometry, using fluorophore-labeled 10.17DT SOSIP trimer tetramers to detect 10.17DT-specific B cells (Figure S4). Both 10.17DT F14 and 113C-429GCG gp160 mRNA-LNP elicited 10.17DT-specific GC B cells and memory B cells (Figure 2F). The average frequencies of 10.17DT-specific GC B cells among total GC B cell population was 1.42% in the 10.17DT F14 gp160 mRNA-LNP group and 0.95% in the 10.17DT 113C-429GCG mRNA-LNP group. The 10.17DT F14 gp160 mRNA-LNP vaccinated group had higher frequencies of 10.17DT-specific memory B cells among total memory B cells compared with the 10.17DT 113C-429GCG gp160 mRNA-LNP vaccinated group (mean at 13.14% versus 3.88%, $p < 0.01$, Exact Wilcoxon Mann-Whitney U test). Additionally, 10.17DT gp160 mRNA-LNP elicited spleen Tfh cell and GC Tfh cell responses in both groups (Figures 2G and S4).

Antigenicity of modified mRNA-encoded CH848 10.17DT SOSIP trimers with stabilizing mutations

The antigenicity of mRNA-expressed *Galanthus nivalis* lectin (GNL)-purified 10.17DT SOSIP trimers was measured by enzyme-linked immunosorbent assay (ELISA) using a panel of bnAbs and nnAbs (Figures 1A and 3A; Table S1). Each stabilized construct encoded by mRNA efficiently bound to V3-glycan bnAbs 2G12, PGT125, PGT128, and DH270 lineage Abs DH270 UCA, DH270 IA4, and DH270.1. In particular, mRNA-encoded 10.17DT DS SOSIP trimers displayed greater binding reactivity to bnAbs compared with other stabilizing mutations. Consistent with our observations with 10.17DT gp160s, the Vt8 and F14/Vt8 mutations decreased DH270 UCA binding to 10.17DT SOSIP trimers. 10.17DT Vt8 and F14/Vt8 SOSIP trimers also displayed lower binding to trimer-specific bnAb PGT151 compared with 10.17DT v4.1, DS, and F14 SOSIP trimers, suggesting less native-like conformation of Envs. Little to non-detectable binding to bnAbs was observed with v5.2.8 and UFO mutations combined (v5.2.8 + UFO). All stabilized constructs tested presented low to non-detectable levels of binding to most nnAbs, except for 10.17DT SOSIPv5.2.8, which displayed about binding to nnAbs 19b and F105 compared with other stabilized Envs tested.

SPR analysis showed that sCD4 treatment of mRNA-expressed non-stabilized 10.17DT SOSIPv4.1 trimers increased binding of nnAb 17b. In contrast, 10.17DT DS, F14, and F14/Vt8 showed low to non-detectable binding to 17b with or without sCD4 treatment. Although 10.17DT Vt8, v5.2.8, and v5.2.8 + UFO trimers exhibited increased binding to 17b after sCD4 treatment, the binding was at a lower response level compared with 10.17DT SOSIPv4.1. Similar trends were observed for 19b binding (Figure 3B).

We next used size exclusion ultra-performance liquid chromatography (SE-UPLC) to define the folding of mRNA-encoded CH848 10.17DT SOSIP trimers. The analytical SE-UPLC profile of bnAb PGT151-purified 10.17DT DS SOSIP trimer protein indicated that a well-folded 10.17DT SOSIP trimer was separated and eluted from the column, as shown in Figure 4A. GNL-purified mRNA-expressed 10.17 DT v4.1 and DS SOSIP trimer samples showed a dominant peak of trimer that was 62% and 65% of the total peak, respectively (Figures 4B and 4C). NSEM analysis of 10.17DT DS trimer confirmed the expression of well-folded SOSIP trimers from mRNA-transfected 293-F supernatant (Figure 4D).

Antigenicity of CH848 10.17DT trimer-ferritin NPs with stabilizing mutations encoded by modified mRNAs

CH848 10.17DT NPs were designed by gene fusion of the 10.17DT SOSIP trimer gene with *Helicobacter pylori* (*H. pylori)* ferritin gene (*FtnA*; GenBank: NP_223316) and were tested for expression, stability, and antigenicity (Figure 5A). Moreover, we asked whether we could further improve the antigenicity and immunogenicity of 10.17DT Env by filling the glycan holes at positions 230 and 289 and by introducing 169K mutation, which is critical to Env interaction with V2-glycan bnAbs (Doria-Rose et al., 2012; Lee et al., 2017; McLellan et al., 2011). This 10.17DT Env trimer (CH848 10.17DT D230N H289N P291S E169K) was termed "enhanced CH848 10.17DT" (CH848 10.17DTe). Since the linker sequence connecting ferritin and Env protein would affect the expression and assembly of NPs, we tested 10.17DTe DS NPs with two different linkers, the sequences of which were GGGSGGGGSGLSK (termed "2xGS linker") and GGGSGGGGSGGGGSGLSK (termed "3xGS linker"). We also designed another NP construct using the *H. pylori* ferritin with a N19Q mutation, which removed a potential N-linked glycosylation site at position 19 and added a glycine and a serine to the C terminus of the ferritin protein ("VRC ferritin") (Kanekiyo et al., 2013).

All CH848 10.17DT and 10.17DTe NPs exhibited effective binding to V3-glycan bnAbs tested (Figure 5B). 10.17DTe NPs displayed robust binding to V2-glycan bnAbs PGT145, PG9, and VRC26.25, while V3-glycan bnAb and DH270 lineage antibody bindings were comparable to 10.17DT with E169, demonstrating that 10.17DTe Envs had improved antigenicity by filling glycan holes and restoring V2-glycan bnAb binding without impairing V3-glycan targeted antibody binding. In contrast, 10.17DT and 10.17DTe NPs showed low to non-detectable binding to nnAbs (Figure 5B). Specifically, none of the NPs showed binding to 17b, and the binding to 19b was low, except for 10.17DT 113C-429GCG NPs, indicative of an exposed distal V3 loop.

SPR analysis following sCD4 treatment showed no increased binding of nnAb 17b to CH848 10.17DT and 10.17DTe NPs and low levels of binding of nnAb 19b (Figure 5C). Thus, 10.17DT NPs could be expressed with mRNAs and bound to bnAbs efficiently

A

Binding reactivities of bnAbs and nnAbs to modified mRNA-expressed CH848 10.17DT SOSIP trimers

	nnAbs								bnAb/bnAb precursors											
	coreceptor	V3		V2		CD4bs		CD4i	DH270 lineage			V3-glycan			V2-glycan					gp41-gp120 interface
Trimers	17b	19b	F39F	CH58	697D	F105	b12	A32	DH270 UCA	DH270 IA4	DH270.1	2G12	PGT125	PGT128	PGT145	CH01	PG9	VRC26.25	PGT151
v4.1	1	2	1	0	3	3	3	1	4	4	4	3	3	7	1	1	1	0	6
DS	0	2	3	0	3	4	1	2	4	4	4	3	3	6	1	2	1	0	6
F14	0	1	1	0	3	1	1	1	3	3	3	2	2	5	1	1	1	0	5
Vt8	0	1	0	0	1	2	1	1	2	2	3	2	5	6	1	1	1	0	4
F14/Vt8	0	1	0	0	2	1	1	1	1	2	3	2	5	6	1	1	1	0	3
v5.2.8	1	3	1	0	2	6	1	0	3	3	3	2	2	5	0	1	1	0	5
v5.2.8+UFO	0	1	0	0	1	1	0	0	0	0	1	1	0	1	0	0	0	0	0

ELISA score	0	1	2	3	4	5	6	7
logAUC	=0	0-1	1-2	2-3	3-4	4-5	5-6	6-7

B

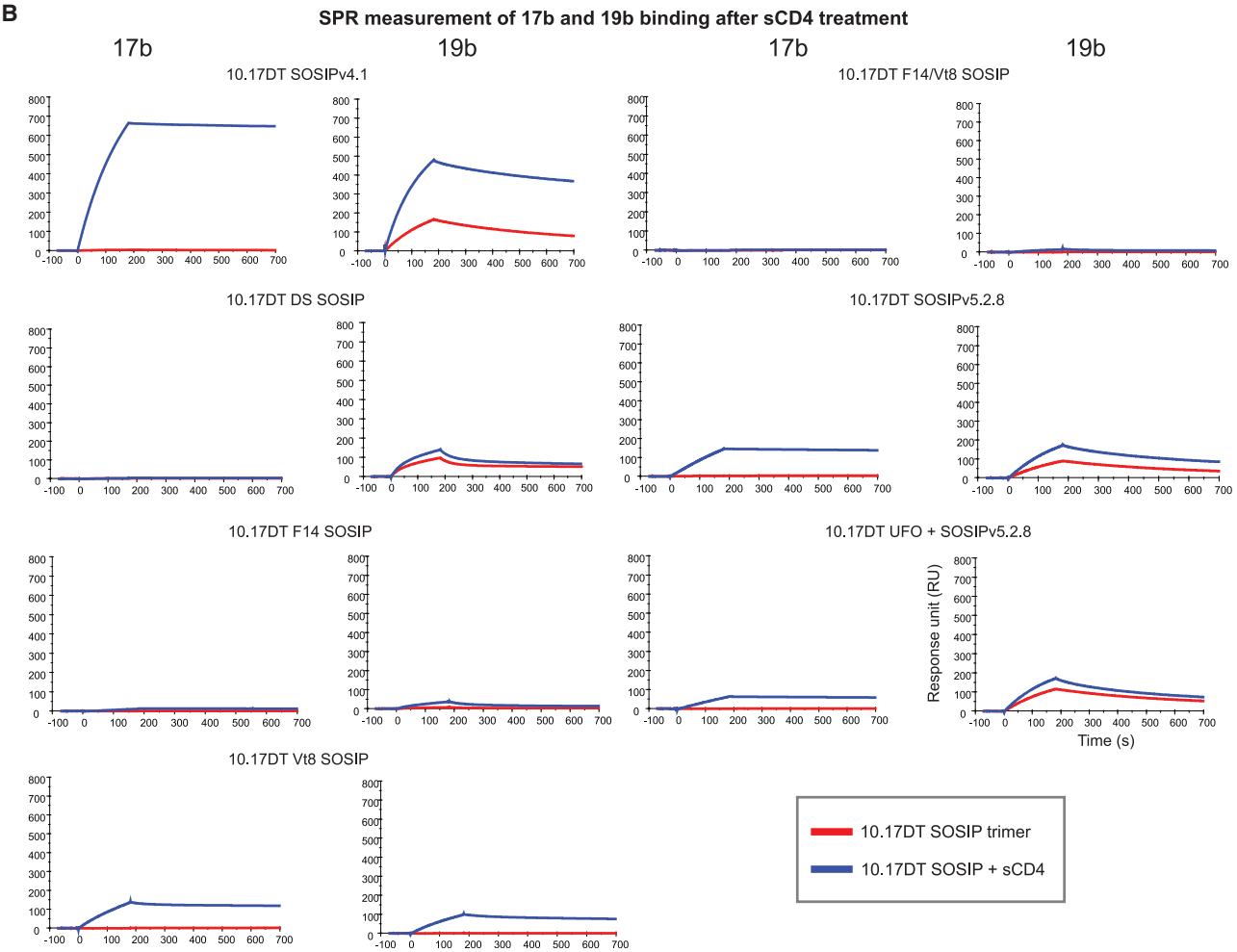

Figure 3. Antigenicity of modified mRNA-encoded CH848 10.17DT SOSIP trimers with stabilizing mutations

(A) BnAb/bnAb precursor and nnAb binding reactivity to mRNA-expressed CH848 10.17DT SOSIP trimers with various stabilizing mutations measured by ELISA. Data shown are means of logAUC from three independent experiments.

(B) SPR sensorgrams of nnAb 17b or 19b binding to mRNA-expressed CH848 10.17DT SOSIP trimers with or without sCD4 treatment.

See also Table S1.

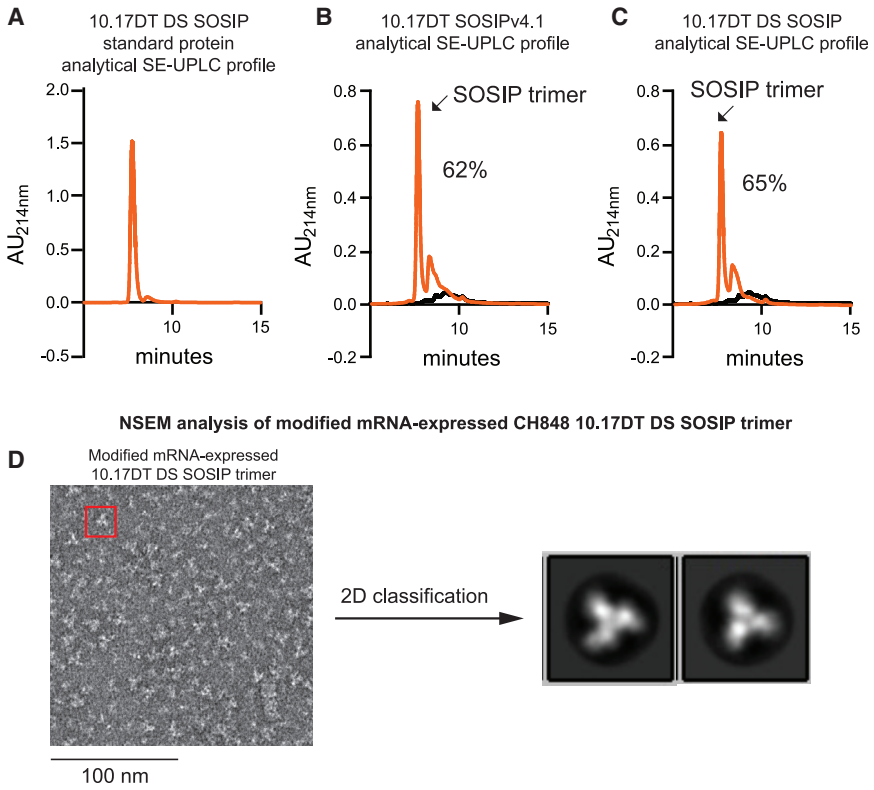

Figure 4. Modified mRNA-expressed CH848 10.17DT DS SOSIP trimer is well folded

(A) Analytical SE-UPLC profile of CH848 10.17DT SOSIP trimer protein standard purified by bnAb PGT151.

(B and C) Analytical SE-UPLC profile of mRNA-expressed GNL-purified (B) CH848 10.17DT SOSIPv4.1 trimers and (C) DS SOSIP trimers. Black curve indicates GNL-purified material from mock transfection.

(D) Negative-stain electron microscopy (NSEM) analysis of mRNA-expressed GNL-purified CH848 10.17DT DS SOSIP trimers. Shown on the left is a representative NSEM micrograph of 10.17DT DS SOSIP trimer; on the right are 2D classification of well-folded trimers.

with limited binding to nnAbs when optimized stabilizing mutations were present.

Furthermore, mRNA-expressed 10.17DT DS SOSIP trimers without ferritin bound to base-binding antibodies DH1029, DH1312, and RM19R IgG. In contrast, DH1029 and DH1312 showed no binding to NPs, while RM19R IgG showed minimal binding to 10.17DT NPs that were lower than binding to trimer alone (Figure 5D).

We assessed whether mRNA-expressed CH848 10.17DT protein indeed self-assembled into NPs by NSEM. We purified mRNA-transfected 293-F supernatants of 10.17DTe DS VRC and 10.17DTe DS 3xGS linker NPs by bnAb PGT145 and demonstrated that both mRNAs produced stabilized, well-folded NPs (Figures 5E and S5). In addition, 2D classification analyses identified free Env trimers, unknown trimeric proteins, proteosome molecules with seven-fold symmetry (Adams, 2003), species in polygon shapes, and small unidentifiable particles (Figure S5). Polygon-shaped particles have been observed in HIV-1 Env protein preparation by others (He et al., 2016) and represent secreted host galectin-3-binding proteins (Gal-3BP) that assemble into ring-like polymers (Muller et al., 1999; Sasaki et al., 1998). Thus, many of these 2D classes were host proteins co-purified with Env proteins. If we considered unknown trimeric proteins as mRNA derived in non-native forms, then well-folded NPs consisted of a minimum of 53.3% and 49.7% of total Env protein particles in 10.17DTe DS 3xGS linker and 10.17DTe DS VRC samples, respectively. If only folded NPs and SOSIP trimers are considered mRNA derived and unknown trimeric proteins host derived, the percentage of well-folded NPs among identifiable NPs and free trimers were 100% for the 10.17DTe DS 3xGS linker NP sample and 64.5% for the 10.17DTe DS VRC NP sample (Figures S5D and S5H).

CH848 10.17DT SOSIP trimer-ferritin NP mRNA-LNP induced autologous tier 2 neutralizing antibodies

To assess the immunogenicity of mRNA-LNP encoding CH848 10.17DT NPs, we immunized DH270 UCA KI mice (Figure 6A). All 10.17DT NP mRNA-LNP elicited serum IgGs bound to 10.17DT trimer and CH848 Δ11 gp120 proteins (Figures 6B, S6A, and S6B). None of the NPs consistantly induced undesired V3 loop peptide or gp41-binding antibodies, suggesting that NPs had stabilization of the V3 loop *in vivo* (Figures 6B, S6C, and S6D). We detected binding activity to *H. pylori* ferritin but did not observe any immunized mouse serum cross-reactivity with human ferritin (Figures S6E and S6F). Since a mouse antibody recognizing human ferritin has been reported (Bayat et al., 2013), the lack of cross-creativity to human ferritin was not due to limited mouse antibody repertoire but indeed suggested antibodies that react with *H. pylori* ferritin do not cross-react to human ferritin. We determined if immunized mouse serum contained antibodies that could block the trimer base-binding antibody DH1029. No blocking of DH1029 binding was observed in 10.17DT NP mRNA-LNP vaccinated mice, except for one mouse vaccinated with 10.17DT 113C-429GCG NP mRNA-LNP. In contrast, sera from a control group of 10.17DT DS SOSIP trimer protein vaccinated DH270 UCA KI mice showed DH1029 blocking activity after the second and third immunizations (Figure 6C). Thus, vaccination with 10.17DT NP mRNA-LNP in DH270 UCA KI mice did not elicit trimer base-targeted antibodies, whereas 10.17DT DS SOSIP trimer protein did.

Next, we assessed tier 2 serum neutralizing antibody titers after three immunizations against a panel of HIV-1 strains in the TZM-bl neutralization assay. All CH848 10.17DT NP mRNA-LNP elicited neutralizing antibodies against autologous tier 2 virus CH848 10.17DT in an N332-dependent manner (Figures 6D

CellPress
OPEN ACCESS

A

Design of CH848 10.17DT trimer-ferritin nanoparticles

B

Binding reactivities of bnAbs and nnAbs to modified mRNA-expressed CH848 10.17DT trimer-ferritin NPs

	nnAbs								bnAbs/bnAb precursors											
	coreceptor	V3		V2		CD4bs		CD4i	DH270 lineage			V3-glycan			V2-glycan				gp41-gp120 interface	
Trimer-ferritin NPs	17b	19b	F39F	CH58	697D	F105	b12	A32	DH270 UCA	DH270 IA4	DH270.1	2G12	PGT125	PGT128	PGT145	CH01	PG9	VRC26.25	PGT151	
10.17DT DS	0	2	1	0	1	3	0	1	2	3	3	2	3	4	0	1	1	0	3	
10.17DTe DS 2xGS linker	0	2	1	1	1	2	0	2	2	3	3	3	4	5	4	2	5	5	3	
10.17DTe DS 3xGS linker	0	1	1	1	1	1	0	1	2	2	3	3	3	5	3	1	4	4	2	
10.17DTe DS VRC	0	2	2	1	1	3	0	2	1	1	2	2	2	4	1	1	4	3	1	
10.17DT 113C-429GCG	0	5	5	0	2	1	2	1	2	2	3	2	3	5	0	0	0	0	3	

ELISA score	0	1	2	3	4	5
logAUC	=0	0-1	1-2	2-3	3-4	4-5

C

SPR measurement of 17b and 19b binding to after sCD4 treatment

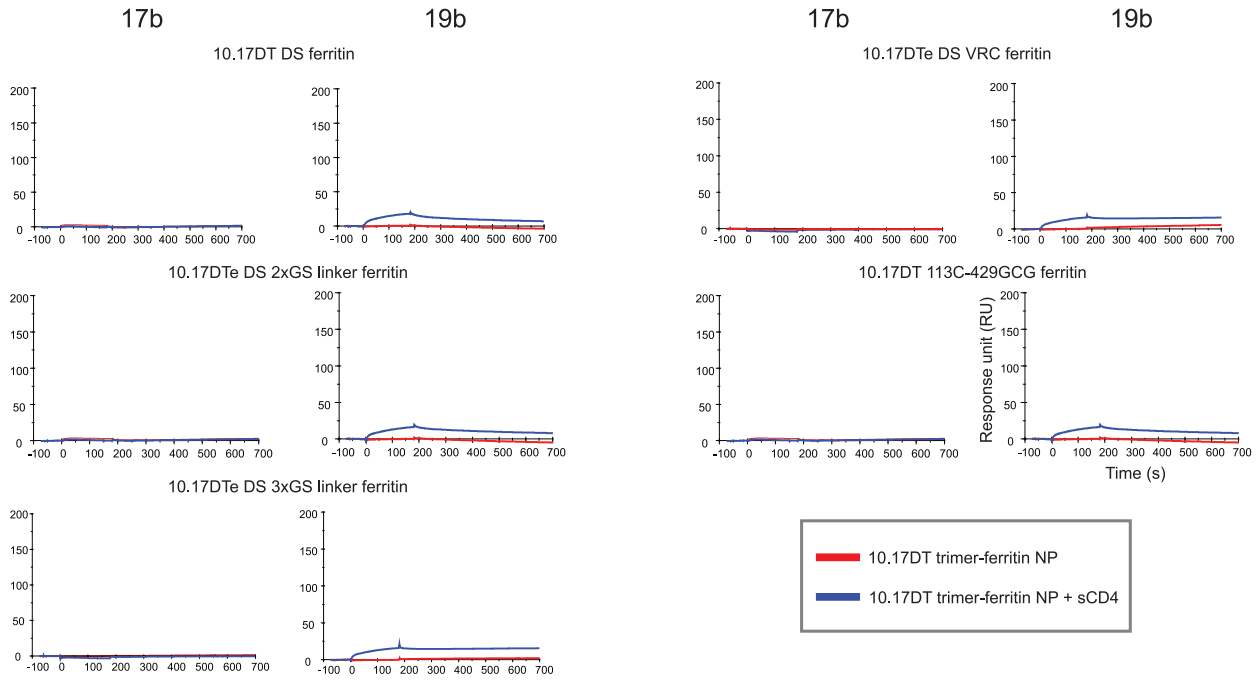

D

Env base antibody binding

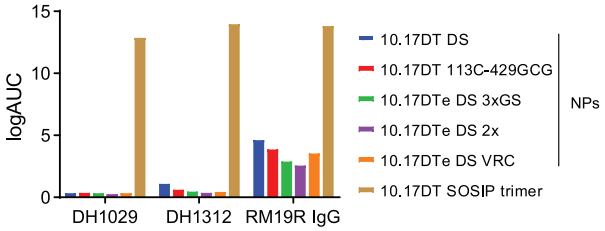

E

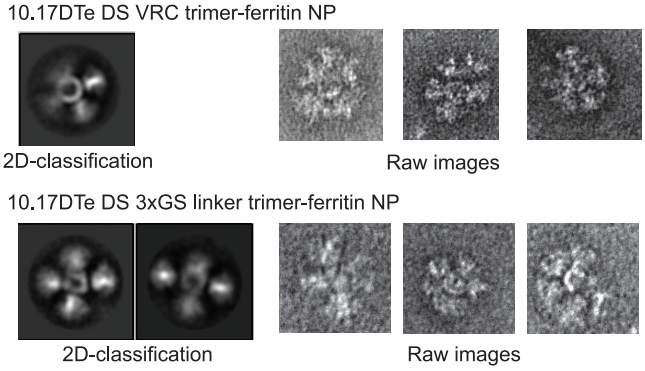

(legend on next page)

and S6G). Comparable neutralizing titers against glycan holes-filled CH848 10.17DT 230N 289N 291S virus were observed, indicating that the antibody responses were not directed at glycan holes but rather were targeted to the V3-glycan bnAb site. 10.17DTe DS VRC NP mRNA-LNP vaccinated mice showed higher neutralizing titers to CH848 10.17DT 230N 289N 291S viruses compared with 10.17DT DS ($p < 0.05$, Exact Wilcoxon Mann-Whitney U test) and 10.17DT 113C-429GCG ($p < 0.01$, Exact Wilcoxon Mann-Whitney U test) NP mRNA-LNP vaccinated groups. Thus, 10.17DT NPs encoded as mRNA-LNP efficiently elicited tier 2 autologous neutralizing antibodies that targeted the N332-dependent V3 glycan bnAb site.

CH848 10.17DT SOSIP trimer-ferritin NP mRNA-LNP elicited germinal center responses and selected for key DH270 bnAb mutations

Each of the five CH848 10.17DT NPs selected the improbable V_H G57R mutation in DH270 UCA KI gene, with the highest median of mutation frequency at 3.2% observed in 10.17DT 113C-429GCG NP vaccinated mice. Similarly, the R98T mutation in the DH270 UCA V_H KI gene was also selected in all groups by mRNA-LNP (Figure 6E). Thus, mRNA-LNP encoded 10.17DT NP immunizations in DH270 UCA KI mice efficiently elicited key improbable mutations.

Each of the five CH848 10.17DT NP mRNA-LNP induced 10.17DT-specific GC B cells and memory B cells in spleens (Figure 6F). Tfh cells and GC Tfh cells were also observed in all 10.17DT NP vaccinated mice (Figure 6G). No significant difference was observed among the five immunization groups ($p < 0.05$, Exact Wilcoxon Mann-Whitney U test). Interestingly, empty LNP immunizations also elicited Tfh cell responses, albeit at a much lower frequency, consistent with previous observations that mRNA-LNP have adjuvant effects that favor Tfh cell and GC responses (Alameh et al., 2021; Pardi et al., 2018a).

CH848 10.17DT trimer-ferritin NP mRNA-LNP immunization induced heterologous neutralizing mAbs that acquired improbable mutations

To further assess antibody responses elicited by CH848 10.17DT NP mRNA-LNP, we injected DH270 UCA KI mice intradermally (i.d.) or intramuscularly (i.m.) with 10.17DT DS NP mRNA-LNP for six immunizations and sorted 10.17DT-specific single memory B cells on 96-well plates and amplified immunoglobulin (Ig) heavy- and light-chain variable regions by PCR (Figures 7A, 7B, and S7). We cloned a total of 397 Ig heavy- and light-chain pairs, 228 (57%) pairs of which used DH270 KI genes *IGVH1-2* and *IGVL2-23*. Among these 228 DH270-like antibodies, 173 (76%) antibodies have acquired at least one amino acid mutation (Figures 7C and S7B). We aligned all unique VH1-2/VL2-23 Ig gene amino acid sequences with bnAb DH270.6 and found that the Ig heavy-chain group accumulated a total of 14 out of 19 (74%) DH270.6 probable mutations and 4 out of 8 (50%) DH270.6 improbable mutations (Figure S8). Similarly, the Ig light-chain group accumulated 6 out of 9 (67%) DH270.6 probable mutations and 4 out of 6 (67%) improbable mutations (Figure S9). Specifically, 5 (2%) and 20 (9%) Ig heavy chains acquired the DH270.6 bnAb G57R and the R98T improbable mutations, respectively, and 2 (1%) Ig light chains acquired the DH270.6 bnAb L48Y improbable mutation. Two Ig heavy chains had both G57R and R98T mutations (Figure 7D). Binding reactivity of cloned antibodies was screened in ELISA (Table S3), and antibodies with heterologous HIV-1 A.Q23 Env binding were selected for further assessment. Among them, three mAbs (DH270.mu84, DH270.mu85, and DH270.mu86) were identified that showed strong binding to CH848 10.17DT, 10.17, and to heterologous HIV-1 A.Q23 SOSIP trimers (Figure 7E). We assessed neutralization of these three mAbs against a panel of 17 HIV-1 isolates that the first intermediate ancestor antibody (DH270 IA4) in the DH270 lineage neutralizes (Figure 7F) (Saunders et al., 2019). Each of the 3 mAbs neutralized autologous tier 2 CH848 viruses and heterologous 92RW020 and 6101.1 viruses with titers comparable to DH270 IA4 (Saunders et al., 2019). Antibody DH270.mu84 also neutralized each of the 13 other heterologous HIV-1 isolates tested. Antibodies DH270.mu85 and DH270.mu86 neutralized 8 and 10 of 13 heterologous isolates, respectively (Figure 7F). DH270.mu84 encoded the V_H G57R improbable mutation, DH270.mu86 encoded the V_H R98T improbable mutation, while DH270.mu85 had both the G57R and R98T improbable mutations. Additionally, DH270.mu86 acquired V_L S27Y and V_L S57N improbable mutations (Figure 7G). One intriguing observation was that DH270.mu84 makes a tyrosine mutation to the "invariant" cysteine that occurs before CDRL1 (C22Y). We hypothesized that the C22Y mutation might enhance DH270.mu84 neutralization potency or breadth due to increased antibody flexibility (Klein et al., 2013). In summary, CH848 10.17DT DS NP mRNA-LNP immunization induced heterologous tier 2 neutralizing DH270 antibodies with improbable mutations.

DISCUSSION

A major question addressed here is whether mRNA designs can incorporate stabilizing mutations in trimers or NPs to optimize immunogen expression and stability since the protein products of mRNAs cannot be purified after mRNA-LNP injection *in vivo*. In this study, we evaluated mutations that stabilize

Figure 5. Antigenicity of CH848 10.17DT trimer-ferritin NPs with stabilizing mutations

(A) Design of CH848 10.17DT SOSIP trimer-ferritin fusion NPs.

(B) BnAb/bnAb precursor and nnAb binding reactivity to mRNA-expressed CH848 10.17DT NPs with various stabilizing mutations measured by ELISA. Data shown are means of logAUC from three independent experiments.

(C) SPR sensorgrams of nnAb 17b or 19b binding to mRNA-expressed CH848 10.17DT NPs with or without sCD4 treatment.

(D) Binding reactivity of Env base antibodies DH1029, DH1312, and RM19R IgG to mRNA-expressed CH848 10.17DT DS SOSIP trimer or CH848 10.17DT NPs measured by ELISA. Data shown are means of logAUC from at least two independent experiments.

(E) Representative NSEM images and 2D classifications of mRNA-expressed, PGT145-purified CH848 10.17DTe DS VRC and 10.17DTe DS 3xGS linker NPs. See also Figures S2 and S5 and Table S1.

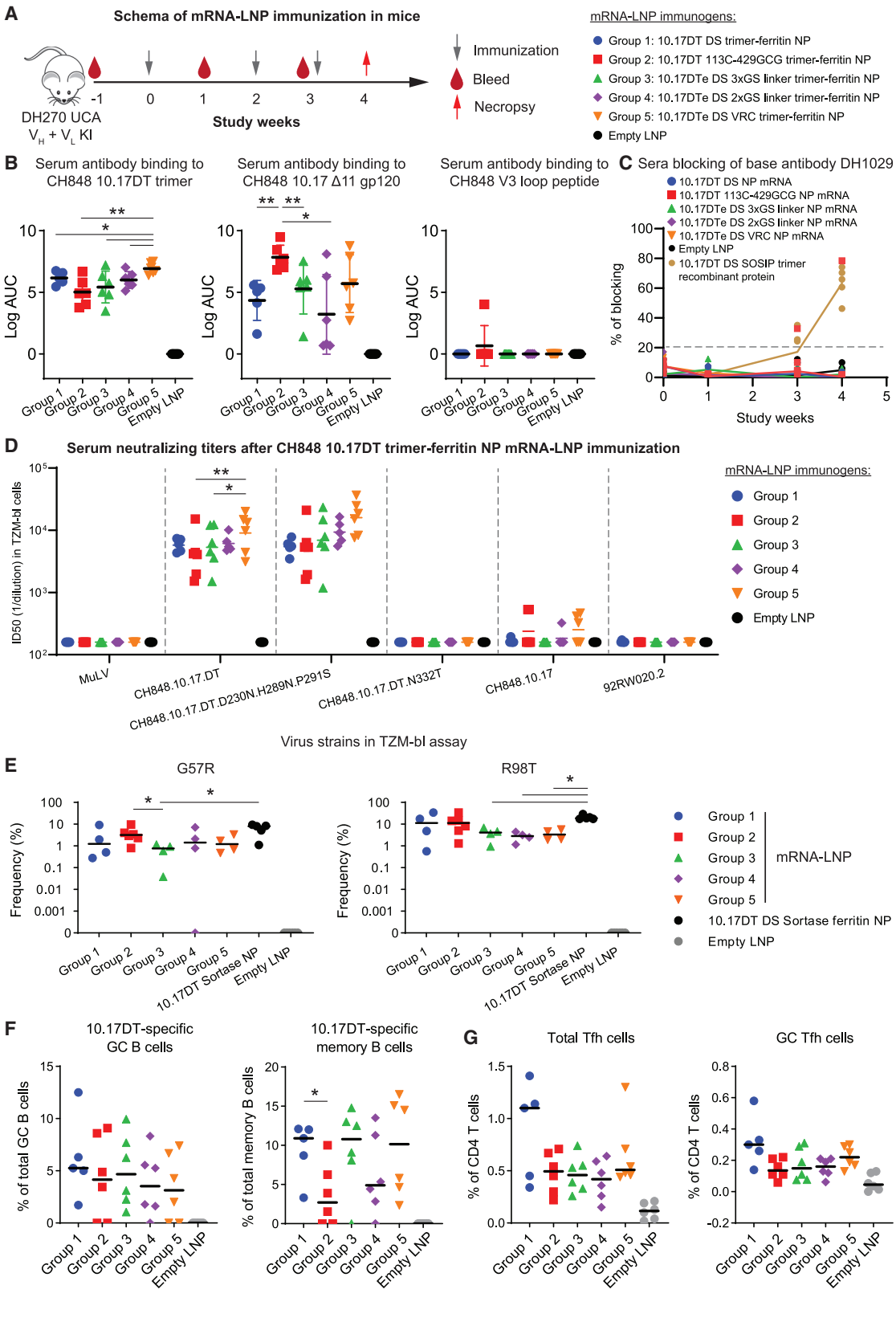

(legend on next page)

mRNA-encoded Envs expressed as transmembrane gp160s, soluble SOSIP trimers, or single-gene mRNA trimer-ferritin NPs. For mRNAs encoding the V3-glycan germline-targeting CH848 10.17DT Env (Saunders et al., 2019), we showed that F14 mutations optimally stabilized transmembrane gp160s, the DS mutations best stabilized SOSIP trimers and NPs expressed from mRNA.

mRNA-LNP encoding both transmembrane gp160s and soluble NPs induced high titers of autologous bnAb-targeted tier 2 neutralizing antibodies with groups of mutations present in bnAb intermediate antibodies in DH270 UCA KI mice (Bonsignori et al., 2017; Saunders et al., 2019). Moreover, we observed accumulation of mature bnAb DH270.6 mutations in vaccine-induced mAbs, although mutations are distributed across all isolated mAbs. The next goal is to have mutations concatenated on the same bnAb B cell clonal lineage members. To achieve this, prolonged GC responses or enhanced recruitment of memory B cells back into GCs will need to be induced by vaccination to allow bnAb lineage B cell BCRs to acquire functional mutation required for full bnAb neutralization breadth.

Therefore, we have promising mRNA-LNP vaccine candidates for priming V3-glycan bnAb DH270 B cell lineage in two different Env forms: as a transmembrane Env gp160 and as an NP. Transmembrane gp160 and NP forms encoded by mRNA-LNPs showed similar immunogenicity in DH270 UCA KI mice. High-avidity protein nanoparticles are concentrated in B cell follicles (Martin et al., 2020; Tokatlian et al., 2019) and activate and recruit low-affinity B cells (Kato et al., 2020). It is intriguing that mRNA-LNP-delivered Env gp160s induced serum neutralization titers and the accumulation of functional improbable bnAb mutations that were comparable to NPs (Figure S10). The success of using immunogens in transmembrane form has been demonstrated by two COVID-19 mRNA-LNP vaccines (Baden et al., 2020; Polack et al., 2020). However, the mechanisms of mRNA-delivered Env transmembrane protein in eliciting B cell responses is less clear. Some studies suggest that B cell recognition of membrane-associated antigens plays a role of concentrating antigens for B cell extraction, processing, and presentation (Carrasco and Batista, 2006).

Several studies published recently explored the use of mRNAs for HIV-1 vaccines in various forms, such as self-amplifying mRNA (Aldon et al., 2021; Melo et al., 2019) or mRNA-encoded virus-like particles (Zhang et al., 2021). These studies highlighted the versatility of mRNA vaccine platform for HIV-1 vaccine development and stressed the need for careful studies to compare and evaluate different mRNA technologies.

Eliciting bnAbs by vaccination has not been successful in humans. However, studies in HIV-1-infected individuals have demonstrated that those who make bnAbs have higher levels of T follicular helper (Tfh) cells (Locci et al., 2013; Moody et al., 2016). Nucleoside-modified mRNA-LNP vaccines selectively induce high levels of Tfh cells (Lederer et al., 2020; Pardi et al., 2018a) and thus will be a key platform to test for bnAb lineage initiation and selection of B cells with improbable functional mutations that facilitate bnAb maturation. The CH848 10.17DTe DS NP is currently in good manufacturing practice (GMP) production to investigate the priming of such lineages in humans both as mRNA-LNPs and as recombinant proteins.

In conclusion, we have demonstrated that single-chain mRNAs can be designed to encode complex molecules and that these immunogens are capable of selecting for difficult-to-elicit improbable mutations critical for broad tier 2 virus neutralization. The complex biology of HIV-1 bnAbs necessitates a vaccine strategy that utilizes a series of sequentially administered Env immunogens that initially expand bnAb precursors and then select for improbable mutations (Haynes et al., 2012, 2019; Saunders et al., 2019; Wiehe et al., 2018). Manufacturing of complex nanoparticle protein immunogens in large scale is faced with significant practical and funding challenges (Mu et al., 2021). The use of mRNA-LNPs raises the possibility of making such a complex immunization regimen both logistically achievable and potentially cost effective.

Limitations of the study

There are several limitations in this study. It is technically challenging to purify modified mRNA-encoded immunogens expressed *in vivo* and evaluate the stability directly. However, Pardi et al. have compared the *in vitro* transfection of HEK293T cells and dendritic cells with mRNA-LNPs and demonstrated mRNA expression in each cell type to be at similar levels (Pardi et al., 2015). Thus, the careful assessment of immune responses in animal models for the induction of "off-target" antibody responses targeting undesired epitopes on destabilized Env proteins is critical. Finally, the assessment of the immunogenicity of mRNA-LNP in this study was performed in the DH270 UCA KI mouse model. Although a valuable tool for testing HIV-1 vaccines, a concern of this model is the relatively high frequency (~10%) of DH270 UCA B cells among the naive B cell repertoire

Figure 6. Immunogenicity of CH848 10.17DT trimer-ferritin NP mRNA-LNP in mice

(A) Immunization schema with CH848 10.17DT NP mRNA-LNP in DH270 UCA KI mice.

(B) Serum IgG binding to CH848 10.17DT SOSIP trimer, 10.17 Δ11 gp120, and V3 peptide. Each dot represents an individual mouse (n = 5 in Group 1; n = 6 in the rest of groups). Horizontal bar, mean. Error bar, SD.

(C) Measurement of serum IgG that block DH1029 binding to CH848 10.17DT SOSIP trimer. 10.17DT DS SOSIP trimer protein vaccinated mice from one of our previous studies were included as positive control. This positive control is the same as that plotted in Figure 2C. Dotted horizontal line, 20% background cut-off.

(D) Serum neutralizing titers after CH848 10.17DT SOSIP NP mRNA-LNP immunization measured in TZM-bl reporter cells. MuLV was used as negative control. Neutralization titers are reported as ID_{50}. Each dot signifies an individual mouse. Horizontal bar, ID_{50} GMT.

(E) Improbable G57R and R98T mutation frequencies in DH270 V_H KI gene after CH848 10.17DT mRNA-LNP immunizations. Frequencies were compared to three CH848 10.17DT Sortase ferritin NP protein immunizations and empty LNP immunizations. Horizontal bar, median.

(F) Frequencies of CH848 10.17DT-specific GC B cells and memory B cells in splenocytes of 10.17DT NP mRNA-LNP vaccinated mice. Horizontal bar, mean.

(G) Frequencies of total Tfh cells and GC Tfh cells in spleen of 10.17DT NP mRNA-LNP vaccinated mice. Horizontal bar, mean. Significance was determined by Exact Wilcoxon Mann-Whitney U test, without any p value adjustment for multiple comparison. *$p < 0.05$, **$p < 0.01$.

See also Figures S4, S6, and S10.

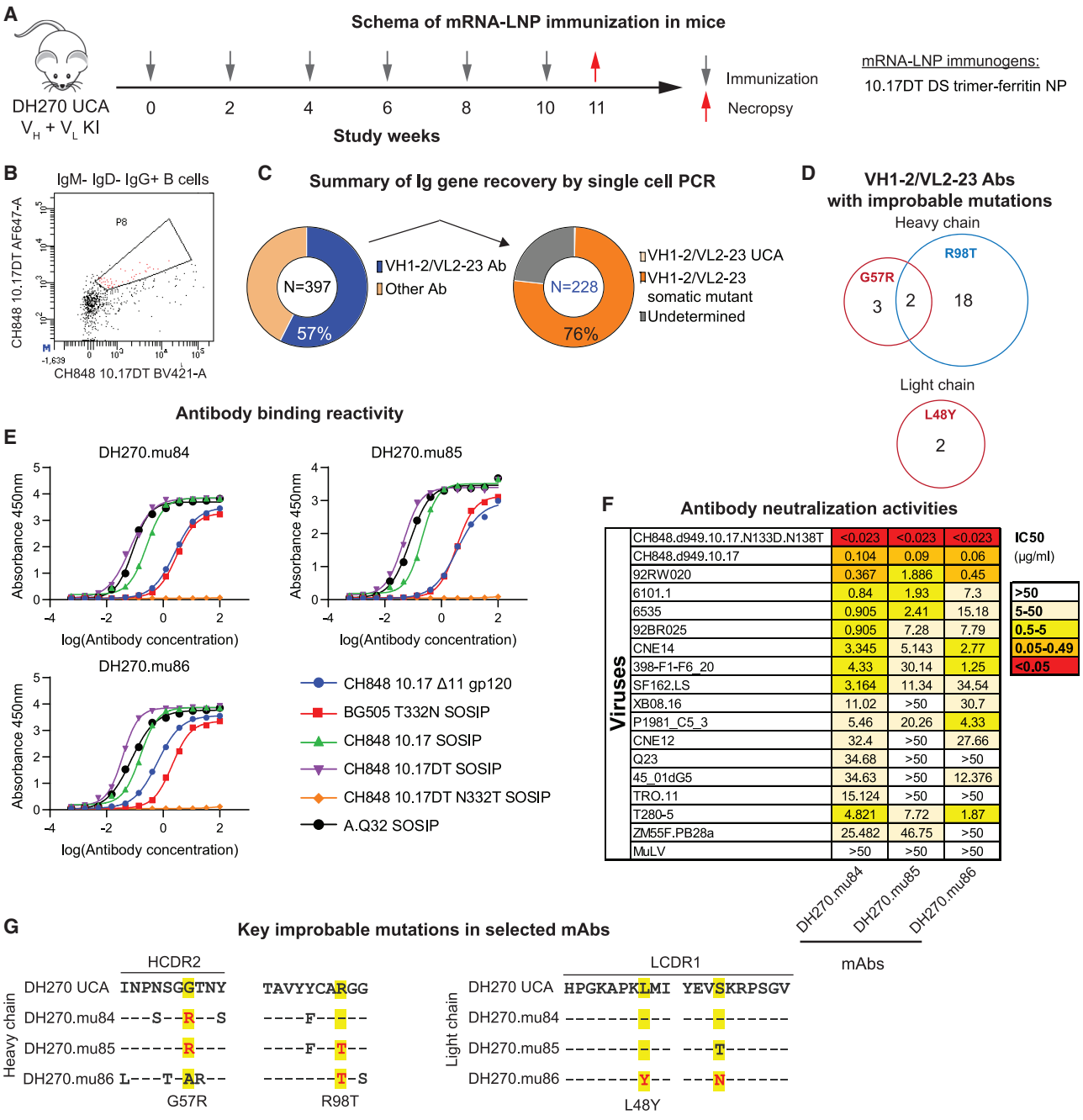

Figure 7. CH848 10.17DT DS trimer-ferritin NP mRNA-LNP vaccination elicited antibodies that acquired improbable mutations and neutralization breadth

(A) Immunization schema with CH848 10.17DT DS NP mRNA-LNP in DH270 UCA KI mice.

(B) Representative gate for CH848 10.17DT Env-specific single memory B cell sorting from DH270 UCA KI mice splenocytes.

(C) Summary of Ig gene recovery by PCR from single-cell sorted memory B cells. Ig gene pairs that used DH270 *IGVH1-2* and *IGVL2-23* genes were considered as DH270-like Abs. Ig gene pairs that used only one of DH270 heavy chain or light chain, or endogenous mouse Ig genes are categorized as "Other Ab". Right: the number and percentage of the 228 DH270-like Abs that had acquired at least one amino acid change in heavy or light chain. VH1-2/VL2-23 Abs without full length, clean VDJ/VJ sequences are categorized as "Undetermined".

(D) Summary of improbable mutations in DH270-like Abs.

(E) Binding reactivity of mAbs DH270.mu84, DH270.mu85, and DH270.mu86 to a panel of HIV-1 Env SOSIP trimer proteins measured by ELISA.

(legend continued on next page)

(Saunders et al., 2019). Future studies in outbred animal models, such as rhesus macaques, will be important to further assess the immunogenicity of mRNA-LNP vaccines.

STAR★METHODS

Detailed methods are provided in the online version of this paper and include the following:

- KEY RESOURCES TABLE
- RESOURCE AVAILABILITY
  - Lead contact
  - Materials availability
  - Data and code availability
- EXPERIMENTAL MODEL AND SUBJECT DETAILS
  - Cell line
  - Animals and immunizations
- METHOD DETAILS
  - Design of CH848 10.17DT Envs with stabilizing mutations
  - Nucleoside-modified mRNA production
  - Nucleoside-modified mRNA-LNP production
  - Nucleoside-modified mRNA transfection in 293-F cell line
  - Evaluation of expression and folding of modified mRNA-expressed CH848 10.17DT gp160s, SOSIP trimers, and trimer-ferritin NPs
  - Mouse serological analysis by ELISA
  - HIV-1 pseudovirus neutralization assay
  - Next-generation sequencing (NGS)
  - Antibody sequence analysis
  - Flow cytometric phenotyping of GC responses
  - Isolation of CH848 10.17DT-specific neutralizing monoclonal antibodies (mAbs)
- QUANTIFICATION AND STATISTICAL ANALYSIS

SUPPLEMENTAL INFORMATION

Supplemental information can be found online at https://doi.org/10.1016/j.celrep.2022.110514.

ACKNOWLEDGMENTS

We thank Holly Zoeller for assistance with SE-UPLC assays; Cindy Bowman, Grace Stevens, and Austin Harner for help with animal studies; Victoria Gee-Lai and Maggie Barr for help with ELISA assays, and Matthew Gardner at Emory University and Michael Farzan at Scripps Research Institute Florida for providing eCD4-Ig. We acknowledge Andrew Ward and Christopher Cottrell at Scripps Research Institute and Marit van Gils at Academisch Medisch Centrum Universiteit van Amsterdam for kindly sharing with us RM19R IgG plasmid. We also thank Cynthia Nagel for project management. This project was supported by NIH, NIAID, Division of AIDS Integrated Preclinical and Clinical AIDS Vaccine Development Grant AI135902 and by NIAID, Division of AIDS Consortia for HIV/AIDS Vaccine Development (CHAVD) Grant UM1AI144371.

AUTHOR CONTRIBUTIONS

Conceptualization, Z.M., K.O.S., D.W., and B.F.H.; Methodology, Z.M., R.P., K.O.S., and B.F.H.; Animal models, F.A., M.T.; Software, S.V. and K.J.W.; Investigation, Z.M., K.J.W., K.O.S., R.H., D.W.C., R.P., D.M., A.E., B.K., K.W., K.M., R.J.E., A.N., X.L., S.X., M.B., D.M., Q.H., S.V., T.E., M.A., W.B.W., N.P., D.W., and B.F.H.; Statistical analysis, Y.W. and W.R.; Writing, Z.M., K.O.S., K.J.W., and B.F.H.; Funding Acquisition, B.F.H.; Resources, Y.T., C.B., N.P., D.W., and B.F.H.; Supervision, B.F.H.

DECLARATION OF INTERESTS

B.F.H., K.O.S., and K.W. have patent applications on some of the concepts and immunogens discussed in this paper.

Received: August 7, 2021
Revised: January 9, 2022
Accepted: February 17, 2022
Published: March 15, 2022

REFERENCES

Abbott, R.K., Lee, J.H., Menis, S., Skog, P., Rossi, M., Ota, T., Kulp, D.W., Bhullar, D., Kalyuzhniy, O., Havenar-Daughton, C., et al. (2018). Precursor frequency and affinity determine B cell competitive fitness in germinal centers, tested with germline-targeting HIV vaccine immunogens. Immunity *48*, 133–146.e6.

Adams, J. (2003). The proteasome: structure, function, and role in the cell. Cancer Treat Rev. *29*, 3–9.

Alameh, M.G., Tombacz, I., Bettini, E., Lederer, K., Sittplangkoon, C., Wilmore, J.R., Gaudette, B.T., Soliman, O.Y., Pine, M., Hicks, P., et al. (2021). Lipid nanoparticles enhance the efficacy of mRNA and protein subunit vaccines by inducing robust T follicular helper cell and humoral responses. Immunity *54*, 2877–2892.e7.

Aldon, Y., McKay, P.F., Moreno Herrero, J., Vogel, A.B., Levai, R., Maisonnasse, P., Dereuddre-Bosquet, N., Haas, H., Fabian, K., Le Grand, R., et al. (2021). Immunogenicity of stabilized HIV-1 Env trimers delivered by self-amplifying mRNA. Mol. Ther. Nucleic Acids *25*, 483–493.

Allaway, G.P., Davis-Bruno, K.L., Beaudry, G.A., Garcia, E.B., Wong, E.L., Ryder, A.M., Hasel, K.W., Gauduin, M.C., Koup, R.A., McDougal, J.S., et al. (1995). Expression and characterization of CD4-IgG2, a novel heterotetramer that neutralizes primary HIV type 1 isolates. AIDS Res. Hum. Retroviruses *11*, 533–539.

Baden, L.R., El Sahly, H.M., Essink, B., Kotloff, K., Frey, S., Novak, R., Diemert, D., Spector, S.A., Rouphael, N., Creech, C.B., et al. (2020). Efficacy and safety of the mRNA-1273 SARS-CoV-2 vaccine. N. Engl. J. Med *384*, 403–416.

Baiersdorfer, M., Boros, G., Muramatsu, H., Mahiny, A., Vlatkovic, I., Sahin, U., and Kariko, K. (2019). A facile method for the removal of dsRNA contaminant from in vitro-transcribed mRNA. Mol. Ther. Nucleic Acids *15*, 26–35.

Bayat, A.A., Yeganeh, O., Ghods, R., Zarnani, A.H., Ardekani, R.B., Mahmoudi, A.R., Mahmoudian, J., Haghighat-Noutash, F., and Jeddi-Tehrani, M. (2013). Production and characterization of a murine monoclonal antibody against human ferritin. Avicenna J. Med. Biotechnol. *5*, 212–219.

Binley, J.M., Sanders, R.W., Master, A., Cayanan, C.S., Wiley, C.L., Schiffner, L., Travis, B., Kuhmann, S., Burton, D.R., Hu, S.L., et al. (2002). Enhancing the proteolytic maturation of human immunodeficiency virus type 1 envelope glycoproteins. J. Virol. *76*, 2606–2616.

(F) DH270.mu84, DH270.mu85, and DH270.mu86 neutralization activity against a panel of 17 HIV-1 isolates. Data shown are antibody concentration that inhibit 50% of virus replication (IC_{50}) in TZM-bl assay. MuLV was used as negative control.
(G) Improbable mutations in mAbs DH270.mu84, DH270.mu85, and DH270.mu86. Alignment of mAb heavy- and light-chain sequences with DH270 UCA sequences. Mutations are highlighted, and improbable mutations are shown in red fonts.
See also Figures S7–S9 and Table S3.

Bonsignori, M., Kreider, E.F., Fera, D., Meyerhoff, R.R., Bradley, T., Wiehe, K., Alam, S.M., Aussedat, B., Walkowicz, W.E., Hwang, K.K., et al. (2017). Staged induction of HIV-1 glycan-dependent broadly neutralizing antibodies. Sci. Transl. Med. *9*, eaai7514.

Bonsignori, M., Zhou, T., Sheng, Z., Chen, L., Gao, F., Joyce, M.G., Ozorowski, G., Chuang, G.Y., Schramm, C.A., Wiehe, K., et al. (2016). Maturation pathway from germline to broad HIV-1 neutralizer of a CD4-mimic antibody. Cell *165*, 449–463.

Bradley, T., Fera, D., Bhiman, J., Eslamizar, L., Lu, X., Anasti, K., Zhang, R., Sutherland, L.L., Scearce, R.M., Bowman, C.M., et al. (2016). Structural constraints of vaccine-induced tier-2 autologous HIV neutralizing antibodies targeting the receptor-binding site. Cell Rep. *14*, 43–54.

Carrasco, Y.R., and Batista, F.D. (2006). B cell recognition of membrane-bound antigen: an exquisite way of sensing ligands. Curr. Opin. Immunol. *18*, 286–291.

Cottrell, C.A., van Schooten, J., Bowman, C.A., Yuan, M., Oyen, D., Shin, M., Morpurgo, R., van der Woude, P., van Breemen, M., Torres, J.L., et al. (2020). Mapping the immunogenic landscape of near-native HIV-1 envelope trimers in non-human primates. PLoS Pathog. *16*, e1008753.

Crooks, E.T., Tong, T., Chakrabarti, B., Narayan, K., Georgiev, I.S., Menis, S., Huang, X., Kulp, D., Osawa, K., Muranaka, J., et al. (2015). Vaccine-elicited tier 2 HIV-1 neutralizing antibodies bind to quaternary epitopes involving glycan-deficient patches proximal to the CD4 binding site. PLoS Pathog. *11*, e1004932.

de Taeye, S.W., Ozorowski, G., Torrents de la Pena, A., Guttman, M., Julien, J.P., van den Kerkhof, T.L., Burger, J.A., Pritchard, L.K., Pugach, P., Yasmeen, A., et al. (2015). Immunogenicity of stabilized HIV-1 envelope trimers with reduced exposure of non-neutralizing epitopes. Cell *163*, 1702–1715.

Doria-Rose, N.A., Georgiev, I., O'Dell, S., Chuang, G.Y., Staupe, R.P., McLellan, J.S., Gorman, J., Pancera, M., Bonsignori, M., Haynes, B.F., et al. (2012). A short segment of the HIV-1 gp120 V1/V2 region is a major determinant of resistance to V1/V2 neutralizing antibodies. J. Virol. *86*, 8319–8323.

Fellinger, C.H., Gardner, M.R., Weber, J.A., Alfant, B., Zhou, A.S., and Farzan, M. (2019). eCD4-Ig limits HIV-1 escape more effectively than CD4-ig or a broadly neutralizing antibody. J. Virol. *93*, e00443.

Guenaga, J., Dubrovskaya, V., de Val, N., Sharma, S.K., Carrette, B., Ward, A.B., and Wyatt, R.T. (2015). Structure-guided redesign increases the propensity of HIV env to generate highly stable soluble trimers. J. Virol. *90*, 2806–2817.

Havenar-Daughton, C., Lee, J.H., and Crotty, S. (2017). Tfh cells and HIV bnAbs, an immunodominance model of the HIV neutralizing antibody generation problem. Immunol. Rev. *275*, 49–61.

Havenar-Daughton, C., Sarkar, A., Kulp, D.W., Toy, L., Hu, X., Deresa, I., Kalyuzhniy, O., Kaushik, K., Upadhyay, A.A., Menis, S., et al. (2018). The human naive B cell repertoire contains distinct subclasses for a germline-targeting HIV-1 vaccine immunogen. Sci. Transl. Med. *10*, eaat0381.

Haynes, B.F., Burton, D.R., and Mascola, J.R. (2019). Multiple roles for HIV broadly neutralizing antibodies. Sci. Transl. Med. *11*, eaaz2686.

Haynes, B.F., Fleming, J., St Clair, E.W., Katinger, H., Stiegler, G., Kunert, R., Robinson, J., Scearce, R.M., Plonk, K., Staats, H.F., et al. (2005). Cardiolipin polyspecific autoreactivity in two broadly neutralizing HIV-1 antibodies. Science *308*, 1906–1908.

Haynes, B.F., Kelsoe, G., Harrison, S.C., and Kepler, T.B. (2012). B-cell-lineage immunogen design in vaccine development with HIV-1 as a case study. Nat. Biotechnol. *30*, 423–433.

Haynes, B.F., Shaw, G.M., Korber, B., Kelsoe, G., Sodroski, J., Hahn, B.H., Borrow, P., and McMichael, A.J. (2016). HIV-host interactions: implications for vaccine design. Cell Host Microbe *19*, 292–303.

He, L., de Val, N., Morris, C.D., Vora, N., Thinnes, T.C., Kong, L., Azadnia, P., Sok, D., Zhou, B., Burton, D.R., et al. (2016). Presenting native-like trimeric HIV-1 antigens with self-assembling nanoparticles. Nat. Commun. *7*, 12041.

Henderson, R., Lu, M., Zhou, Y., Mu, Z., Parks, R., Han, Q., Hsu, A.L., Carter, E., Blanchard, S.C., Edwards, R.J., et al. (2020). Disruption of the HIV-1 Envelope allosteric network blocks CD4-induced rearrangements. Nat. Commun. *11*, 520.

Hraber, P., Seaman, M.S., Bailer, R.T., Mascola, J.R., Montefiori, D.C., and Korber, B.T. (2014). Prevalence of broadly neutralizing antibody responses during chronic HIV-1 infection. AIDS *28*, 163–169.

Huang, D., Abbott, R.K., Havenar-Daughton, C., Skog, P.D., Al-Kolla, R., Groschel, B., Blane, T.R., Menis, S., Tran, J.T., Thinnes, T.C., et al. (2020). B cells expressing authentic naive human VRC01-class BCRs can be recruited to germinal centers and affinity mature in multiple independent mouse models. Proc. Natl. Acad. Sci. U S A *117*, 22920–22931.

Jardine, J., Julien, J.P., Menis, S., Ota, T., Kalyuzhniy, O., McGuire, A., Sok, D., Huang, P.S., MacPherson, S., Jones, M., et al. (2013). Rational HIV immunogen design to target specific germline B cell receptors. Science *340*, 711–716.

Jayaraman, M., Ansell, S.M., Mui, B.L., Tam, Y.K., Chen, J., Du, X., Butler, D., Eltepu, L., Matsuda, S., Narayanannair, J.K., et al. (2012). Maximizing the potency of siRNA lipid nanoparticles for hepatic gene silencing in vivo. Angew. Chem. Int. Ed. Engl. *51*, 8529–8533.

Kanekiyo, M., Wei, C.J., Yassine, H.M., McTamney, P.M., Boyington, J.C., Whittle, J.R., Rao, S.S., Kong, W.P., Wang, L., and Nabel, G.J. (2013). Self-assembling influenza nanoparticle vaccines elicit broadly neutralizing H1N1 antibodies. Nature *499*, 102–106.

Kato, Y., Abbott, R.K., Freeman, B.L., Haupt, S., Groschel, B., Silva, M., Menis, S., Irvine, D.J., Schief, W.R., and Crotty, S. (2020). Multifaceted effects of antigen valency on B cell response composition and differentiation in vivo. Immunity *53*, 548–563.e8.

Klein, F., Diskin, R., Scheid, J.F., Gaebler, C., Mouquet, H., Georgiev, I.S., Pancera, M., Zhou, T., Incesu, R.B., Fu, B.Z., et al. (2013). Somatic mutations of the immunoglobulin framework are generally required for broad and potent HIV-1 neutralization. Cell *153*, 126–138.

Kong, L., He, L., de Val, N., Vora, N., Morris, C.D., Azadnia, P., Sok, D., Zhou, B., Burton, D.R., Ward, A.B., et al. (2016). Uncleaved prefusion-optimized gp140 trimers derived from analysis of HIV-1 envelope metastability. Nat. Commun. *7*, 12040.

Kwon, Y.D., Pancera, M., Acharya, P., Georgiev, I.S., Crooks, E.T., Gorman, J., Joyce, M.G., Guttman, M., Ma, X., Narpala, S., et al. (2015). Crystal structure, conformational fixation and entry-related interactions of mature ligand-free HIV-1 Env. Nat. Struct. Mol. Biol. *22*, 522–531.

Lederer, K., Castano, D., Gomez Atria, D., Oguin, T.H., 3rd, Wang, S., Manzoni, T.B., Muramatsu, H., Hogan, M.J., Amanat, F., Cherubin, P., et al. (2020). SARS-CoV-2 mRNA vaccines foster potent antigen-specific germinal center responses associated with neutralizing antibody generation. Immunity *53*, 1281–1295.e5.

Lee, J.H., Andrabi, R., Su, C.Y., Yasmeen, A., Julien, J.P., Kong, L., Wu, N.C., McBride, R., Sok, D., Pauthner, M., et al. (2017). A broadly neutralizing antibody targets the dynamic HIV envelope trimer apex via a long, rigidified, and anionic beta-hairpin structure. Immunity *46*, 690–702.

Lee, J.H., Hu, J.K., Georgeson, E., Nakao, C., Groschel, B., Dileepan, T., Jenkins, M.K., Seumois, G., Vijayanand, P., Schief, W.R., et al. (2021). Modulating the quantity of HIV Env-specific CD4 T cell help promotes rare B cell responses in germinal centers. J. Exp. Med. *218*, e20201254.

Liao, H.X., Levesque, M.C., Nagel, A., Dixon, A., Zhang, R.J., Walter, E., Parks, R., Whitesides, J., Marshall, D.J., Hwang, K.K., et al. (2009). High-throughput isolation of immunoglobulin genes from single human B cells and expression as monoclonal antibodies. J. Virol. Methods *158*, 171–179.

Locci, M., Havenar-Daughton, C., Landais, E., Wu, J., Kroenke, M.A., Arlehamn, C.L., Su, L.F., Cubas, R., Davis, M.M., Sette, A., et al. (2013). Human circulating PD-1+CXCR3-CXCR5+ memory Tfh cells are highly functional and correlate with broadly neutralizing HIV antibody responses. Immunity *39*, 758–769.

Maier, M.A., Jayaraman, M., Matsuda, S., Liu, J., Barros, S., Querbes, W., Tam, Y.K., Ansell, S.M., Kumar, V., Qin, J., et al. (2013). Biodegradable lipids enabling rapidly eliminated lipid nanoparticles for systemic delivery of RNAi therapeutics. Mol. Ther. *21*, 1570–1578.

Martin, J.T., Cottrell, C.A., Antanasijevic, A., Carnathan, D.G., Cossette, B.J., Enemuo, C.A., Gebru, E.H., Choe, Y., Viviano, F., Fischinger, S., et al. (2020). Targeting HIV Env immunogens to B cell follicles in nonhuman primates through immune complex or protein nanoparticle formulations. NPJ Vaccin. *5*, 72.

Mascola, J.R., D'Souza, P., Gilbert, P., Hahn, B.H., Haigwood, N.L., Morris, L., Petropoulos, C.J., Polonis, V.R., Sarzotti, M., and Montefiori, D.C. (2005). Recommendations for the design and use of standard virus panels to assess neutralizing antibody responses elicited by candidate human immunodeficiency virus type 1 vaccines. J. Virol. *79*, 10103–10107.

McCoy, L.E., van Gils, M.J., Ozorowski, G., Messmer, T., Briney, B., Voss, J.E., Kulp, D.W., Macauley, M.S., Sok, D., Pauthner, M., et al. (2016). Holes in the glycan shield of the native HIV envelope are a target of trimer-elicited neutralizing antibodies. Cell Rep. *16*, 2327–2338.

McGuire, A.T., Dreyer, A.M., Carbonetti, S., Lippy, A., Glenn, J., Scheid, J.F., Mouquet, H., and Stamatatos, L. (2014). HIV antibodies. Antigen modification regulates competition of broad and narrow neutralizing HIV antibodies. Science *346*, 1380–1383.

McGuire, A.T., Hoot, S., Dreyer, A.M., Lippy, A., Stuart, A., Cohen, K.W., Jardine, J., Menis, S., Scheid, J.F., West, A.P., et al. (2013). Engineering HIV envelope protein to activate germline B cell receptors of broadly neutralizing anti-CD4 binding site antibodies. J. Exp. Med. *210*, 655–663.

McLellan, J.S., Pancera, M., Carrico, C., Gorman, J., Julien, J.P., Khayat, R., Louder, R., Pejchal, R., Sastry, M., Dai, K., et al. (2011). Structure of HIV-1 gp120 V1/V2 domain with broadly neutralizing antibody PG9. Nature *480*, 336–343.

Melo, M., Porter, E., Zhang, Y., Silva, M., Li, N., Dobosh, B., Liguori, A., Skog, P., Landais, E., Menis, S., et al. (2019). Immunogenicity of RNA replicons encoding HIV env immunogens designed for self-assembly into nanoparticles. Mol. Ther. *27*, 2080–2090.

Moody, M.A., Pedroza-Pacheco, I., Vandergrift, N.A., Chui, C., Lloyd, K.E., Parks, R., Soderberg, K.A., Ogbe, A.T., Cohen, M.S., Liao, H.X., et al. (2016). Immune perturbations in HIV-1-infected individuals who make broadly neutralizing antibodies. Sci. Immunol. *1*, aag0851.

Mu, Z., Haynes, B.F., and Cain, D.W. (2021). HIV mRNA vaccines-progress and future paths. Vaccines *9*, 134.

Muller, S.A., Sasaki, T., Bork, P., Wolpensinger, B., Schulthess, T., Timpl, R., Engel, A., and Engel, J. (1999). Domain organization of Mac-2 binding protein and its oligomerization to linear and ring-like structures. J. Mol. Biol. *291*, 801–813.

Pancera, M., Lai, Y.T., Bylund, T., Druz, A., Narpala, S., O'Dell, S., Schon, A., Bailer, R.T., Chuang, G.Y., Geng, H., et al. (2017). Crystal structures of trimeric HIV envelope with entry inhibitors BMS-378806 and BMS-626529. Nat. Chem. Biol. *13*, 1115–1122.

Pardi, N., Hogan, M.J., Naradikian, M.S., Parkhouse, K., Cain, D.W., Jones, L., Moody, M.A., Verkerke, H.P., Myles, A., Willis, E., et al. (2018a). Nucleoside-modified mRNA vaccines induce potent T follicular helper and germinal center B cell responses. J. Exp. Med. *215*, 1571–1588.

Pardi, N., Hogan, M.J., Pelc, R.S., Muramatsu, H., Andersen, H., DeMaso, C.R., Dowd, K.A., Sutherland, L.L., Scearce, R.M., Parks, R., et al. (2017). Zika virus protection by a single low-dose nucleoside-modified mRNA vaccination. Nature *543*, 248–251.

Pardi, N., Muramatsu, H., Weissman, D., and Kariko, K. (2013). In vitro transcription of long RNA containing modified nucleosides. Methods Mol. Biol. *969*, 29–42.

Pardi, N., Parkhouse, K., Kirkpatrick, E., McMahon, M., Zost, S.J., Mui, B.L., Tam, Y.K., Kariko, K., Barbosa, C.J., Madden, T.D., et al. (2018b). Nucleoside-modified mRNA immunization elicits influenza virus hemagglutinin stalk-specific antibodies. Nat. Commun. *9*, 3361.

Pardi, N., Tuyishime, S., Muramatsu, H., Kariko, K., Mui, B.L., Tam, Y.K., Madden, T.D., Hope, M.J., and Weissman, D. (2015). Expression kinetics of nucleoside-modified mRNA delivered in lipid nanoparticles to mice by various routes. J. Control. Release *217*, 345–351.

Pincus, S.H., Fang, H., Wilkinson, R.A., Marcotte, T.K., Robinson, J.E., and Olson, W.C. (2003). In vivo efficacy of anti-glycoprotein 41, but not anti-glycoprotein 120, immunotoxins in a mouse model of HIV infection. J. Immunol. *170*, 2236–2241.

Polack, F.P., Thomas, S.J., Kitchin, N., Absalon, J., Gurtman, A., Lockhart, S., Perez, J.L., Perez Marc, G., Moreira, E.D., Zerbini, C., et al. (2020). Safety and efficacy of the BNT162b2 mRNA covid-19 vaccine. N. Engl. J. Med. *383*, 2603–2615.

Sahin, U., Muik, A., Derhovanessian, E., Vogler, I., Kranz, L.M., Vormehr, M., Baum, A., Pascal, K., Quandt, J., Maurus, D., et al. (2020). COVID-19 vaccine BNT162b1 elicits human antibody and TH1 T cell responses. Nature *586*, 594–599.

Sasaki, T., Brakebusch, C., Engel, J., and Timpl, R. (1998). Mac-2 binding protein is a cell-adhesive protein of the extracellular matrix which self-assembles into ring-like structures and binds beta 1 integrins, collagens and fibronectin. EMBO J. *17*, 1606–1613.

Saunders, K.O., Pardi, N., Parks, R., Santra, S., Mu, Z., Sutherland, L., Scearce, R., Barr, M., Eaton, A., Hernandez, G., et al. (2021). Lipid nanoparticle encapsulated nucleoside-modified mRNA vaccines elicit polyfunctional HIV-1 antibodies comparable to proteins in nonhuman primates. NPJ Vaccin. *6*, 50.

Saunders, K.O., Verkoczy, L.K., Jiang, C., Zhang, J., Parks, R., Chen, H., Housman, M., Bouton-Verville, H., Shen, X., Trama, A.M., et al. (2017). Vaccine induction of heterologous tier 2 HIV-1 neutralizing antibodies in animal models. Cell Rep. *21*, 3681–3690.

Saunders, K.O., Wiehe, K., Tian, M., Acharya, P., Bradley, T., Alam, S.M., Go, E.P., Scearce, R., Sutherland, L., Henderson, R., et al. (2019). Targeted selection of HIV-specific antibody mutations by engineering B cell maturation. Science *366*, eaay7199.

Steichen, J.M., Lin, Y.C., Havenar-Daughton, C., Pecetta, S., Ozorowski, G., Willis, J.R., Toy, L., Sok, D., Liguori, A., Kratochvil, S., et al. (2019). A generalized HIV vaccine design strategy for priming of broadly neutralizing antibody responses. Science *366*, eaax4380.

Tokatlian, T., Read, B.J., Jones, C.A., Kulp, D.W., Menis, S., Chang, J.Y.H., Steichen, J.M., Kumari, S., Allen, J.D., Dane, E.L., et al. (2019). Innate immune recognition of glycans targets HIV nanoparticle immunogens to germinal centers. Science *363*, 649–654.

Tran, E.E., Borgnia, M.J., Kuybeda, O., Schauder, D.M., Bartesaghi, A., Frank, G.A., Sapiro, G., Milne, J.L., and Subramaniam, S. (2012). Structural mechanism of trimeric HIV-1 envelope glycoprotein activation. PLoS Pathog. *8*, e1002797.

Turner, H.L., Andrabi, R., Cottrell, C.A., Richey, S.T., Song, G., Callaghan, S., Anzanello, F., Moyer, T.J., Abraham, W., Melo, M., et al. (2021). Disassembly of HIV envelope glycoprotein trimer immunogens is driven by antibodies elicited via immunization. Sci. Adv. *7*, eabh2791.

Wagh, K., Kreider, E.F., Li, Y., Barbian, H.J., Learn, G.H., Giorgi, E., Hraber, P.T., Decker, T.G., Smith, A.G., Gondim, M.V., et al. (2018). Completeness of HIV-1 envelope glycan shield at transmission determines neutralization breadth. Cell Rep. *25*, 893–908.e7.

Ward, A.B., and Wilson, I.A. (2017). The HIV-1 envelope glycoprotein structure: nailing down a moving target. Immunol. Rev. *275*, 21–32.

Wiehe, K., Bradley, T., Meyerhoff, R.R., Hart, C., Williams, W.B., Easterhoff, D., Faison, W.J., Kepler, T.B., Saunders, K.O., Alam, S.M., et al. (2018). Functional relevance of improbable antibody mutations for HIV broadly neutralizing antibody development. Cell Host Microbe *23*, 759–765.e6.

Williams, W.B., Meyerhoff, R.R., Edwards, R.J., Li, H., Manne, K., Nicely, N.I., Henderson, R., Zhou, Y., Janowska, K., Mansouri, K., et al. (2021). Fab-dimerized glycan-reactive antibodies are a structural category of natural antibodies. Cell *184*, 2955–2972.e5.

Zhang, P., Gorman, J., Geng, H., Liu, Q., Lin, Y., Tsybovsky, Y., Go, E.P., Dey, B., Andine, T., Kwon, A., et al. (2018). Interdomain stabilization impairs CD4 binding and improves immunogenicity of the HIV-1 envelope trimer. Cell Host Microbe *23*, 832–844.e6.

Zhang, P., Narayanan, E., Liu, Q., Tsybovsky, Y., Boswell, K., Ding, S., Hu, Z., Follmann, D., Lin, Y., Miao, H., et al. (2021). A multiclade env-gag VLP mRNA vaccine elicits tier-2 HIV-1-neutralizing antibodies and reduces the risk of heterologous SHIV infection in macaques. Nat. Med. *27*, 2234–2245.

Zhang, R., Verkoczy, L., Wiehe, K., Munir Alam, S., Nicely, N.I., Santra, S., Bradley, T., Pemble, C.W.t., Zhang, J., Gao, F., et al. (2016). Initiation of immune tolerance-controlled HIV gp41 neutralizing B cell lineages. Sci. Transl. Med. *8*, 336ra362.

STAR★METHODS

KEY RESOURCES TABLE

REAGENT or RESOURCE	SOURCE	IDENTIFIER
Antibodies		
Goat F(ab')2 Anti-Human IgG - (Fab')2 (PE)	Abcam	Cat#ab98606; RRID:AB_10672217
FITC Rat Anti-Mouse IgG1, Clone A85-1	BD Biosciences	Cat#553443; RRID:AB_394862
FITC Rat Anti-IgG2a/IgG2b, Clone R2-40	BD Biosciences	Cat#553399; RRID:AB_394837
FITC Rat Anti-Mouse IgG3, Clone R40-82	BD Biosciences	Cat#553403; RRID:AB_394840
PerCP/Cyanine5.5 anti-mouse CD21/CD35 (CR2/CR1) antibody	Biolegend	Cat#123416; RRID:AB_1595490
PE anti-MU/HU GL7 Antigen (T/B Cell Act. Marker) antibody	Biolegend	Cat#144608; RRID:AB_2562926
PE-CF594 Rat Anti-Mouse CD93 (Early B Lineage) Clone AA4.1	BD Biosciences	Cat#563805; RRID:AB_2738431
PE/Cyanine5 anti-mouse TER-119/Erythroid Cells antibody	Biolegend	Cat#116210; RRID:AB_313711
PE-Cy7 Rat Anti-IgM, Clone R6-60.2	BD Biosciences	Cat#552867; RRID:AB_394500
APC-R700 Rat Anti-Mouse CD19 Clone 1D3	BD Biosciences	Cat#565473; RRID:AB_2739253
BV510 Rat Anti-Mouse IgD Clone 11-26C.1	BD Biosciences	Cat#563110; RRID:AB_2737003
BV605 Hamster Anti-Mouse CD95 Clone Jo2	BD Biosciences	Cat#740367; RRID:AB_2740099
BV650 Rat Anti-Mouse CD45R/B220 Clone RA3-6B2	BD Biosciences	Cat#563893; RRID:AB_2738471
BV711 Rat Anti-Mouse CD138 Clone 281-2	BD Biosciences	Cat#563193; RRID:AB_2631190
BV786 Rat Anti-Mouse CD23 Clone B3B4	BD Biosciences	Cat#563988; RRID:AB_2738526
FITC Rat Anti-Mouse CD4 Clone RM4-5	BD Biosciences	Cat#553047; RRID:AB_394583
PE Rat anti-Mouse CD25 Clone 7D4	BD Biosciences	Cat#558642; RRID:AB_1645250
PE-CF594 Hamster Anti-Mouse CD279 (PD-1) Clone J43	BD Biosciences	Cat#562523; RRID:AB_2737634
PE-Cy7 Rat Anti-Mouse CD62L Clone MEL-14	BD Biosciences	Cat#560516; RRID:AB_1645257
Biotin Rat Anti-Mouse CD185 (CXCR5) Clone 2G8	BD Biosciences	Cat#551960; RRID:AB_394301
APC-R700 Rat Anti-Mouse CD8a Clone 53-6.7	BD Biosciences	Cat#564983; RRID:AB_2739032
BV421 Rat Anti-Mouse CD127 Clone SB/199	BD Biosciences	Cat#566300; RRID:AB_2739672
BV510 Hamster Anti-Mouse CD3e Clone 145-2C11	BD Biosciences	Cat#563024; RRID:AB_2737959
BV570 anti-mouse/human CD11b Antibody, Clone M1/70	Biolegend	Cat#101233; RRID:AB_10896949
BV605 Rat Anti-Mouse CD90.2 Clone 53-2.1	BD Biosciences	Cat#563008; RRID:AB_2665477
Brilliant Violet 650™ anti-mouse NK-1.1 Antibody, Clone PK136	Biolegend	Cat#108736; RRID:AB_2563159
BV711 Rat Anti-Mouse CD44 Clone IM7	BD Biosciences	Cat#563971; RRID:AB_2738518
Goat polyclonal Secondary Antibody to Rabbit IgG - H&L (HRP)	Abcam	Cat# ab97080; RRID:AB_10679808
Mouse Anti-Monkey IgG-HRP	SouthernBiotech	Cat# 4700-05; RRID:AB_2796069
High Sensitivity Streptavidin-HRP	Thermo Fisher Scientific	N/A
Chemicals, peptides, and recombinant proteins		
Galanthus Nivalis Lectin (GNL), Agarose bound	Vector Laboratories	Cat#AL-1243
Streptavidin, AF647 conjugate	Thermo Fisher Scientific	Cat#S21374; RRID:AB_2336066

(*Continued on next page*)

Continued

REAGENT or RESOURCE	SOURCE	IDENTIFIER
m1-pseudouridine-5′-triphosphate	TriLink	Cat#N-1081
CleanCap	TriLink	Cat#N-7413
HIV Env recombinant protein	This paper	N/A
Critical commercial assays		
TransIT-mRNA Transfection Kit	Mirus	Cat#MIR2250
LIVE/DEAD Fixable Aqua Dead Cell Stain Kit	Thermo Fisher Scientific	Cat#L34957
SureBlue Reserve TMB 1-Component Microwell Peroxidase Substrate	Seracare	Cat#5120-0083
RNeasy Mini Kit	Qiagen	Cat#74104
SMARTer Mouse BCR IgG H/K/L Profiling Kit	Takara	Cat#634422
AMPure XP	Beckman Coulter	Cat#A63881
MiSeq Reagent Kit v3 (600 cycle)	Illumina	Cat#MS-102-3003
LIVE/DEAD™ Fixable Near-IR Dead Cell Stain Kit	Thermo Fisher Scientific	Cat#L34975
Experimental models: Cell lines		
Freestyle 293-F cell	Thermo Fisher Scientific	Cat#R79007
Human cell line TZM-bl	NIH ARRRP	Cat#8129
Experimental models: Organisms/strains		
Heterozygous ($VH^{+/-}$, $VL^{+/-}$) DH270 UCA knock-in mouse	Saunders et al., 2019	N/A
Recombinant DNA		
See Table S2 for plasmids used for *in vitro* transcription of modified mRNAs	This paper	N/A
Software and algorithms		
FACSDIVA	BD Biosciences	N/A
FlowJo version 10	BD Biosciences	N/A
Prism version 9	GraphPad Software	N/A

RESOURCE AVAILABILITY

Lead contact

Further information and requests for resources and reagents should be directed to and will be fulfilled by the lead contact, Barton F. Haynes (barton.haynes@duke.edu).

Materials availability

New plasmids generated in this paper will be shared by the lead contact upon request.

Data and code availability

- Original data reported in this paper will be shared by the lead contact upon request.
- This paper did not generate original code.
- Any additional information required to reanalyze the data reported in this paper is available from the lead contact upon request.

EXPERIMENTAL MODEL AND SUBJECT DETAILS

Cell line

Freestyle 293-F cell line (Thermo Fisher Scientific, Cat# R79007) was purchased from Thermo Fisher and cultured in Freestyle 293 Expression Medium (Thermo Fisher Scientific, Cat# 12338-026). Cells were maintained in 8% CO_2 at 37°C at a density between 0.3 × 10^6/mL to 3 × 10^6/mL. Mycoplasma test was performed when a new stock vial was thawed at Duke University Cell Culture Facility.

Animals and immunizations

The DH270 UCA KI mice has been previously described (Saunders et al., 2019). For CH848 10.17DT gp160 mRNA-LNP immunizations, 8-12 weeks old mice were used. 12 DH270 UCA KI mice were split into two groups (N = 6 each group), each group had at least one female mice. Mice were immunized intramuscularly (i.m.) with 20 μg of mRNA-LNP encoding CH848 10.17DT F14 gp160 and

CH848 10.17DT 113C-429GCG gp160 every two weeks for three times. For CH848 10.17DT DS NP immunizations, 6-12 weeks old mice were used, and each group had at least two female mice. Immunizations were performed similarly, except that the second and the third immunizations were only one week apart. Control group mice were injected with 20 μg of empty LNP. Bleeding was performed one week after each immunization. Necropsy was performed one week after the third immunization and blood, spleen, and lymph nodes were collected. All mice were cared for in a facility accredited by the Association for Assessment and Accreditation of Laboratory Animal Care International (AAALAC). All study protocol and all veterinarian procedures were approved by the Duke University Institutional Animal Care and Use Committee (IACUC).

METHOD DETAILS

Design of CH848 10.17DT Envs with stabilizing mutations

Ten stabilization designs were tested in nucleoside-modified mRNA-encoded CH848 10.17DT Envs as transmembrane gp160s, soluble SOSIP trimers, or trimer-ferritin NPs (Figures 1A and Table S1). The DS mutations introduce a disulfide bond in the closed Env trimer and prevents CD4-triggered exposure of the CCR5 co-receptor binding site and the V3 loop (Kwon et al., 2015). The F14 mutations are designed based on a structure of BG505 SOSIP trimer complexed with BMS-626529, a small molecule that blocks soluble CD4 (sCD4)-induced Env rearrangements (Pancera et al., 2017) and stabilize the SOSIP trimer by decoupling the allosteric conformational changes triggered by CD4 binding (Henderson et al., 2020). Vt8 mutations stabilize the V3 loop in the prefusion, V1/V2-coupled state (Henderson et al., 2020). The 113C-429GCG and 113C-431GCG mutations link the Env gp120 subunit inner and outer domains through a neo-disulfide bond, resulting in prefusion stabilized Env trimer with impaired CD4 binding (Zhang et al., 2018). For soluble gp140 trimer stabilization, we also tested SOSIPv4.1, v5.2.8 and uncleaved prefusion-optimized (UFO) mutations. Mutations in v4.1 introduce hydrophobic amino acids to disfavor solvent exposure of the V3 loop and modify gp41 in the SOSIP.664 trimer, which improve trimer formation and thermostability and decrease V3 loop exposure (de Taeye et al., 2015). The UFO design replaces the bend between alpha helices in HR1 with a computationally designed linker and aims to minimize the metastability of HIV-1 gp140 trimer (Kong et al., 2016). Mutations in the v5.2.8 design are designed based upon v4.1 and combine an additional disulfide bond and eight trimer-derived mutations that stabilize BG505 SOSIP trimers (Guenaga et al., 2015). Both v4.1 and v5.2.8 include an improved hexa-arginine furin cleavage site R6 (Binley et al., 2002).

Nucleoside-modified mRNA production

Modified mRNAs were produced by *in vitro* transcription using T7 RNA polymerase (Megascript, Ambion) on linearized plasmids encoding codon-optimized CH848 10.17DT gp160s, CH848 10.17DT SOSIP trimers, or CH848 10.17DT trimer-ferritin NPs. All the HIV-1 modified mRNA constructs used in this study and their corresponding plasmids were listed in Table S2. One-methylpseudouridine (m1Ψ)-5′-triphosphate (TriLink, Cat# N-1081), instead of UTP was used to produce nucleoside-modified mRNAs. Modified mRNAs contain 101 nucleotide-long polyadenylation tails for optimized expression. Modified CH848 10.17DT SOSIPv4.1 trimer and CH848 10.17DT SOSIPv5.2.8 trimer mRNAs were capped using ScriptCap m7G capping system and ScriptCap 2′-O-methyl-transferase kit (ScriptCap, CellScript) (Pardi et al., 2013). Capping of all other *in vitro* transcribed mRNAs was performed co-transcriptionally using the trinucleotide cap1 analog, CleanCap (TriLink, Cat# N-7413). All mRNAs were purified by cellulose purification, as described (Baiersdorfer et al., 2019). All mRNAs were analyzed by agarose gel electrophoresis and were stored frozen at −20°C.

Nucleoside-modified mRNA-LNP production

Nucleoside-modified mRNAs were encapsulated in LNP for mouse immunizations as previously described (Jayaraman et al., 2012; Maier et al., 2013). Modified mRNAs in aqueous phase were rapidly mixed with a solution of lipids dissolved in ethanol. LNP formulation contains ionizable cationic lipid (proprietary to Acuitas)/phosphatidylcholine/cholesterol/PEG-lipid. The cationic lipid and LNP composition are described in US patent US10,221,127.

Nucleoside-modified mRNA transfection in 293-F cell line

293-F cells were diluted to 0.7 × 10^6 cells/mL 24 h before transfection. On the next day, cells were diluted again to 1 × 10^6/mL and seeded into tissue culture plates for transfection. 3 μg of mRNAs expressing gp160s were transfected into 6 mL of cells. For soluble SOSIP trimers, 30 mL of cells were transfected with 12 μg of SOSIP-expressing mRNAs and 3 μg of Furin mRNAs. Transfection volume were doubled to 60 mL for trimer-ferritin NPs. TransIT-mRNA Transfection Kit (Mirus Cat# MIR2250) was used for mRNA transfection following the manufacturer's instructions. Transfected cells were cultured at 37°C with 8% CO_2 and shaking at 120 rpm for 48 h (for gp160) or 72 h (for SOSIP trimers and trimer-ferritin NPs) before harvest.

Evaluation of expression and folding of modified mRNA-expressed CH848 10.17DT gp160s, SOSIP trimers, and trimer-ferritin NPs

The expression and folding of modified mRNA-encoded CH848 10.17DT transmembrane gp160s, Soluble SOSIP trimers, and trimer-ferritin NPs were defined as follows. For CH848 10.17DT transmembrane gp160s, flow cytometry was used to measure binding of a panel of bnAbs and nnAbs. BnAb binding reactivity indicated successful expression of gp160 Envs on cell surface with desired antigenicity. Binding of nnAbs 17b and 19b measured the ability of various stabilizing mutations to keep the gp160 Envs in prefusion

conformation and to decrease the exposure of non-neutralizing epitopes CCR5 binding site and distal V3 loop. Additionally, 7B2 binding was used to measure the exposure of gp41.

For CH848 10.17DT soluble trimer, total Env forms were purified by *Galanthus nivalis* lectin (GNL) from modified mRNA-transfected 293-F cell supernatant. A panel of nnAbs and bnAbs were used in ELISA to measure the expression of non-neutralizing and neutralizing epitopes. Binding of nnAbs 17b and 19b after CD4 triggering were measured by SPR. To assess the percent of trimeric Envs in GNL-purified materials, size-exclusion ultra-performance liquid chromatography (SE-UPLC) analysis was performed with PGT151 affinity-purified CH848 10.17DT SOSIP trimer as a standard. Finally, Negative-stain Electron Microscopy (NSEM) analysis was performed to confirm trimer formation in GNL-purified 293-F transfection supernatant.

Similar antigenicity measurement and SPR analysis was performed on GNL-purified 293-F cell supernatant transfected with modified mRNA expressing CH848 10.17DT trimer-ferritin NPs to evaluate the expression of well-folded Env trimers on the ferritin nanoparticle. Additionally, transfected 293-F supernatant were affinity purified with PGT145-conjugated beads, which exclude host glycan proteins that may be purified by GNL. PGT145-purified materials were analyzed by NSEM to confirm the assembly of CH848 10.17DT DS ferritin NPs.

Flow cytometry

Binding of bnAbs to CH848 10.17DT gp160s was performed by flow cytometry as previously described (Henderson et al., 2020; Saunders et al., 2021). Briefly, modified mRNA-transfected 293-F cells were harvested 48 h after transfection and were washed once with 1% BSA in PBS. Then, cells were incubated with 10 μg/mL of bnAbs in V-bottom 96-well plates for 30 min at 4°C. Cells were then washed with 1% BSA in PBS and incubated with Goat F(ab')2 Anti-Human IgG - (Fab')2 (PE) (Abcam Cat# ab98606, RRID:AB_10672217) for 30 min at 4°C in dark. Then, cells were washed once with PBS and dead cells were stained with LIVE/DEAD Fixable Aqua Dead Cell Stain Kit (Invitrogen Cat# L34957, 1:1000 dilution in PBS) for 15 min at 4°C in dark, then washed twice and re-suspended in 1% BSA in PBS. Flow cytometric data were acquired on a LSRII High-throughput system using FACSDIVA software (BD Biosciences) and were analyzed with FlowJo software (FlowJo). The percentage of 293-F cells that were PE positive was shown in the results.

Measurement of binding of nnAbs after CD4 treatment has been described previously (Henderson et al., 2020). Briefly, mRNA-transfected 293-F cells were first incubated with 20 μg/mL of soluble CD4 (sCD4), eCD4-Ig or CD4-IgG2 for 10 min at 4°C. Cells were washed once with 1% BSA in PBS and then incubated with 10 μg/mL of nnAbs 17b, 19b or 7B2 for 30 min at 4°C. Then, cells were incubated with Goat F(ab')2 Anti-Human IgG - (Fab')2 (PE) and dead cells were stained with LIVE/DEAD Fixable Aqua Dead Cell Stain Kit. Data acquisition and analysis were the same as described above.

Galanthus nivalis lectin purification of SOSIP trimers and trimer-ferritin NPs

293-F cells transfected with modified mRNAs expressing SOSIP trimers or trimer-ferritin NPs were harvested 72 h after transfection and were centrifuged for 30 min at 3000 rpm to remove cells and debris. Supernatant were first filtered using a 0.22 μm vacuum filter and were then concentrated by 50-fold using 10 kDa MWCO concentrators. Concentrated supernatant was incubated with 200 μL of agarose bound *Galanthus nivalis* lectin (GNL) (Vector Laboratories Cat# AL-1243) with gentle rotation at 4°C overnight. The next day, GNL agarose beads were washed with MES wash buffer (20 mM MES, 130 mM NaCl, 10 mM $CaCl_2$ pH 7.0) for three times, and SOSIP trimers or trimer-ferritin NPs were eluted by 500 mM Methyl alpha-D-mannopyranoside in MES wash buffer. The eluates were then dialyzed to 10 mM Tris-HCl pH8 500 mM NaCl using 30kDa MWCO spin concentrators. GNL-purified SOSIP trimers or trimer-ferritin NPs were snap-freezed and stored in −80°C.

Enzyme-linked immunosorbent assay (ELISA)

Binding reactivity of modified mRNA-expressed CH848 10.17DT SOSIP trimers and trimer-ferritin NPs to bnAbs and nnAbs was measured by enzyme-linked immunosorbent assay (ELISA). In brief, HIV-1 antibodies were coated onto 384-well assay plates in 0.1M Sodium bicarbonate overnight at 4°C. GNL-purified SOSIP trimers or trimer-ferritin NPs with serial dilutions were then captured on the plates. Next, poly-serum from CH848 10.17DT-immunized rhesus macaque was incubated for 1 h at room temperature. Then, Mouse Anti-Monkey IgG-HRP (SouthernBiotech Cat# 4700-05, RRID:AB_2796069) was incubated for 1 h at room temperature and plates were developed with SureBlue Reserve TMB 1-Component Microwell Peroxidase Substrate (Seracare Cat# 5120-0083) for 15 min and were stopped with 1% HCl solution. Absorbance at 450 nm were determined by SpectraMax Plus 384 microplate reader (Molecular Devices) and log area-under-curve (log AUC) were calculated using Prism (Graphpad) and shown in figures.

The base binding antibody assay was performed similarly. Briefly, base binding antibody DH1029 was coated onto plates to capture samples. Then, a rabbit serum was incubated before detection with Goat polyclonal Secondary Antibody to Rabbit IgG - H&L (HRP) (Abcam Cat# ab97080, RRID:AB_10679808). The plate development, data acquisition, and analysis were the same as described above.

Size-exclusion ultra-performance liquid chromatography (SE-UPLC)

Size exclusion chromatography of modified mRNA-expressed GNL-purified CH848 10.17DT SOSIP trimers was performed using a Waters Acquity H-Class Bio UPLC System with a Waters Acquity UPLC BEH SEC 450Å, 2.5 μm, 4.6 × 150 mm column (Waters Corporation). An isocratic elution with a mobile phase of 20 mM sodium phosphate 300 mM NaCl pH 7.4, and a flow rate of 0.2 mL/min, was used for the analysis with a quaternary pump. Samples and protein standards were maintained at 5–8°C in the auto-sampler rack prior to injection at a volume of 10 μL. Samples and protein standards with a concentration greater than 1.0 mg/mL were diluted to a down to 1.0 mg/mL using Type 1 water. The column temperature was set to 30°C with detection at a wavelength of 214 nm using a photodiode array detector.

Negative-stain electron microscopy (NSEM)

Negative-stain electron microscopy (NESM) analysis of modified mRNA-expressed CH848 10.17DT SOSIP trimers and trimer-ferritin NPs were performed as previously described (Saunders et al., 2017; Williams et al., 2021).

Surface plasmon resonance (SPR)

SPR analyses of modified mRNA-expressed SOSIP proteins incubated with and without sCD4 against distal V3 loop antibody 19b and CCR5 binding site antibody 17b were obtained using the Biacore S200 instrument (Cytiva). Antibodies 19b and 17b were immobilized onto a CM3 sensor chip to a level of 2000-4000RU. A negative control Influenza IgG1 antibody (CH65) was also immobilized onto the sensor chip for reference subtraction. Modified mRNA-expressed GNL-purified CH848 10.17DT SOSIP trimers or trimer-ferritin NPs were diluted down in HBS-N 1x running buffer to 0.5–2.0 μg and incubated with a 2-8× higher dose of soluble CD4 (4.4 μg) (Progenics Therapeutics). Proteins incubated with and without sCD4 were injected over the sensor chip surface using the High performance injection type for 180s at 30 μL/min. The protein was then allowed to dissociate for 600s followed by sensor surface regeneration of two 20 s injections of glycine pH 2.0 at a flow rate of 50 μL/min. Results were analyzed using the BIAevaluation Software (Cytiva). Protein binding to the CH65 immobilized sensor surface as well as buffer binding were used for double reference subtraction to account for non-specific protein binding and signal drift.

Mouse serological analysis by ELISA

Serum IgG antigen binding assay

Serum IgG binding to HIV-1 antigens was measured by ELISA as previously described (Saunders et al., 2019).

DH1029 blocking assay

DH1029 blocking by vaccinated mouse sera was performed in ELISA. Briefly, 384-well assay plate were coated with 2 μg/mL PGT145. Then, 0.125 μg/mL of CH848 10.17DT E169K SOSIP trimer were captured for 1 h at room temperature. Next, mouse sera at 1:50 dilution or DH1029 mAb in serial dilution (2-fold dilution starting at 2 ug/mL) were incubated for 1 h. Next, biotinylated DH1029 were added to the plate at 0.05 μg/mL for 1 h and binding were detected by High Sensitivity Streptavidin-HRP (Thermo Fisher Scientific, Cat #21130). Plate development and data acquisition were the same as described above.

HIV-1 pseudovirus neutralization assay

Neutralization assays were performed in TZM-bl reporter cells as described (Mascola et al., 2005). The analyses of possible glycan holes on CH848 10.17DT Env was performed using method described before (Wagh et al., 2018). Potential glycan holes were found at amino acid positions 230 and 289. To restore glycosylation at these two sites, Asparagine (N) mutations at positions 230 and 289 (230N 289N) were made. In addition, a Serine (S) mutation at position 291 (291S) was made to complete the NXT/S glycosylation sequence.

Next-generation sequencing (NGS)

We performed next-generation sequencing (NGS) on mouse antibody heavy and light chain variable genes using an Illumina sequencing platform. First, RNA was purified from splenocytes using a RNeasy Mini Kit (Qiagen, Cat# 74,104). Purified RNA was quantified via Nanodrop (Thermo Fisher Scientific) and used to generate Illumina-ready heavy and light chain sequencing libraries using the SMARTer Mouse BCR IgG H/K/L Profiling Kit (Takara, Cat# 634,422). Briefly, 1 μg of total purified RNA from splenocytes was used for reverse transcription with Poly dT provided in the SMARTer Mouse BCR kit for cDNA synthesis. Heavy and light chain genes were then separately amplified using a 5′ RACE approach with reverse primers that anneal in the mouse IgG constant region for heavy chain genes and IgK for the light chain genes (SMARTer Mouse BCR IgG H/K/L Profiling Kit). The DH270 UCA KI mouse model has the light chain gene knocked into the kappa locus, therefore kappa primers provided in the SMARTer Mouse BCR kit were used for light chain gene library preparation. 5 μL of cDNA was used for heavy and light chain gene amplification via two rounds of PCR; PCR1 used 18 cycles and PCR2 used 12 cycles. During PCR2, Illumina adapters and indexes were added. Illumina-ready sequencing libraries were then purified and size-selected by AMPure XP (Beckman Coulter, Cat# A63881) using kit recommendations. The heavy and light chain libraries per mouse were indexed separately, thus allowing us to deconvolute the mouse-specific sequences during analysis. Libraries were quantified using QuBit Fluorometer (Thermo Fisher). Mice were pooled by groups for sequencing on the Illumina MiSeq Reagent Kit v3 (600 cycle) (Illumina, Cat# MS-102-3003) using read lengths of 301/301 with 20% PhiX.

Antibody sequence analysis

NGS data analysis and the analysis of improbable mutation frequencies was performed as described (Wiehe et al., 2018). Animals with <1000 NGS reads likely reflect technical errors during NGS library preparation and thus were excluded from analysis.

Flow cytometric phenotyping of GC responses

For immunophenotyping of murine B cells and Tfh cells, spleens from immunized mice one week after the third immunization were processed into single-cell suspensions and treated with ACK lysis buffer to remove red blood cells. Splenocytes (2×10^6) were suspended in 100 μL PBS/2% FBS. To detect antigen-specific B cells, fluorochrome-mAb conjugates and fluorochrome-conjugated CH848 10.17DT Envs were prepared as a master mix at 2× concentration, then 100 μL of 2× master mix was added to an equal volume of cells (Figure S4). Staining for T cell subsets was conducted in the same manner, with the additional step for detection

of biotinylated mAb with Streptavidin–APC. Cells were incubated at 4°C for 20 minutes, then washed with PBS. Cells were resuspended in 100 μL PBS containing Near-IR Live/Dead (Thermo Fisher Scientific) at 1:1000, and incubated at room temperature for 20 min. Cells were washed in PBS/2% FBS, then re-suspended in PBS/2% formaldehyde. Cells were analyzed on a BD LSRII (BD Biosciences). Data were analyzed using FlowJo v10 (FlowJo).

Isolation of CH848 10.17DT-specific neutralizing monoclonal antibodies (mAbs)

Antibody cloning, screening, and mAbs expression

Immunoglobulin (Ig) gene were cloned from sorted single B cells as previously described (Liao et al., 2009). Briefly, complementary DNA (cDNA) of Ig genes were amplified by reverse-transcription with SuperScript III First-Strand Synthesis System (Thermo Fisher Scientific, Cat# 18080051) using random hexamer oligonucleotides as primers. Ig gene cDNA was then used as template in nested PCR for heavy and light chain gene amplification using AmpliTaq Gold 360 Master Mix (Thermo Fisher Scientific, Cat #4398881). Mouse Ig-specific primers and DH270 variable region-specific primers were used to amplify mouse endogenous Ig genes and DH270 KI Ig genes. Agarose gel electrophoresis was used to identify positive PCR amplification and Ig genes were recovered by Sanger sequencing. Following sequencing, contigs of PCR amplicon sequences were assembled, and Ig genes were inferred with human Ig gene library and mouse Ig gene library in Cloanalyst. PCR reactions with successful Ig sequence recovery were purified using AMPure XP kit (Beckman Coulter, Cat# A63881). Purified PCR product was used for overlapping PCR to generate a linear antibody expression cassette. The expression cassette was transiently transfected with into 293i cells with ExpiFectamine 293 Transfection Kit (Thermo Fisher Scientific, Cat# A14525). The supernatant was harvested 72 h after transfection and screened in ELISA binding assays with a panel of protein of interests. The genes of selected heavy chains were synthesized with human IgG1 backbone (GenScript). Kappa and lambda chains were synthesized similarly. To express mAbs plasmids were prepared for transient transfection using the Plasmid Plus Mega Kit (Qiagen, Cat #12981). Heavy and light chain plasmids were co-transfected into 293i cells using ExpiFectamine 293 Transfection Kit for antibody production.

QUANTIFICATION AND STATISTICAL ANALYSIS

Exact Wilcoxon Mann-Whitney U tests were performed without any adjustment for multiple comparisons. Significant results were indicated in figures and figure legends as: * $P < 0.05$; ** $P < 0.01$.